THE ANATOMICAL RECORD 296:395–413 (2013)

The Role of Cross-Sectional Geometry, Curvature, and Limb Posture in Maintaining Equal Safety Factors: A Computed Tomography Study

CHARLOTTE A. BRASSEY,[1] ANDREW C. KITCHENER,[2,3] PHILIP J. WITHERS,[4] PHILLIP L. MANNING,[5] AND WILLIAM I. SELLERS[1]*

[1]Faculty of Life Sciences, University of Manchester, Manchester, United Kingdom
[2]Department of Natural Sciences, National Museum of Scotland, Edinburgh, United Kingdom
[3]Institute of Geography, School of Geosciences, University of Edinburgh, Drummond Street, Edinburgh, United Kingdom
[4]Henry Moseley X-Ray Imaging Facility, School of Materials, University of Manchester, Manchester, United Kingdom
[5]School of Earth, Atmospheric and Environmental Sciences, University of Manchester, Manchester, United Kingdom

ABSTRACT

The limb bones of an elephant are considered to experience similar peak locomotory stresses as a shrew. "Safety factors" are maintained across the entire range of body masses through a combination of robusticity of long bones, postural variation, and modification of gait. The relative contributions of these variables remain uncertain. To test the role of shape change, we undertook X-ray tomographic scans of the leg bones of 60 species of mammals and birds, and extracted geometric properties. The maximum resistible forces the bones could withstand before yield under compressive, bending, and torsional loads were calculated using standard engineering equations incorporating curvature. Positive allometric scaling of cross-sectional properties with body mass was insufficient to prevent negative allometry of bending (F_b) and torsional maximum force (F_t) (and hence decreasing safety factors) in mammalian (femur $F_b \propto M_b^{0.76}$, $F_t \propto M_b^{0.80}$; tibia $F_b \propto M_b^{0.80}$, $F_t \propto M_b^{0.76}$) and avian hindlimbs (tibiotarsus $F_b \propto M_b^{0.88}$, $F_t \propto M_b^{0.89}$) with the exception of avian femoral F_b and F_t. The minimum angle from horizontal a bone must be held while maintaining a given safety factor under combined compressive and bending loads increases with M_b, with the exception of the avian femur. Postural erectness is shown as an effective means of achieving stress similarity in mammals. The scaling behavior of the avian femur is discussed in light of unusual posture and kinematics. Anat Rec, 296:395–413, 2013. © 2013 Wiley Periodicals, Inc.

Key words: safety factors; effective mechanical advantage (EMA); posture; force; cross-sectional geometry

Grant sponsor: Henry Moseley X-Ray Imaging Facility; Grant numbers: EP/F007906 and EP/I02249X. Grant sponsor: Natural Environment Research Council Doctoral Training Grant; Grant numbers: NE/1528134/1.

*Correspondence to: Charlotte A. Brassey, Faculty of Life Sciences, University of Manchester, Manchester M13 9PL, United Kingdom. E-mail: charlotte.brassey-2@postgrad.manchester.ac.uk

Received 25 May 2012; Accepted 16 December 2012.
DOI 10.1002/ar.22658
Published online 5 February 2013 in Wiley Online Library (wileyonlinelibrary.com).

In engineering terms, the "factor of safety" of a structure is the ratio of its failure strength to the maximum stress it is likely to encounter (Alexander, 1989). This term is also applied in animal biomechanics, reflecting the margin of safety present in vertebrate long bones (Alexander, 1981). Long-bone safety factors experimentally recorded during a range of routine activities such as running and jumping of mammals and birds spanning several orders of magnitude in body mass are remarkably similar, with the ratio of the bone yield stress to the peak stress varying from 1.4 to 4.1 (Rubin and Lanyon, 1982; Biewener, 1983). This relatively narrow range of values can be explained by a number of factors. First, the deposition of skeletal material is subject to strong selective pressures, and safety factors reflect a compromise between optimal stiffness and minimal weight. Not only must bone be grown and maintained, but also accelerated and decelerated through each stride during locomotion, and it is therefore adaptive to minimize the mass of bone wherever possible (Currey, 2003). Second, other physiological constraints also contribute to the ultimate geometry of long bones, such as their functioning as calcium reservoirs and stores of hematopoietic tissues. Third, the basic tetrapod body plan is highly conserved and bone material properties are relatively consistent throughout the evolution of vertebrates (Erickson et al., 2002). These factors would all tend to restrict the range of values of observed safety factors.

Limb safety factors are probably maintained across species via a combination of osteological, behavioral and postural modifications. If animals scaled their support structures isometrically, stress would increase in proportion to body mass$^{1/3}$. However, scaling exponents calculated for cross-sectional bone parameters are consistently above those predicted by isometry for various groups of birds and mammals (Cubo and Casinos, 1998; Garcia and da Silva, 2006). Therefore, several alternative scaling models have been formulated, in which structural support elements are posited to scale allometrically to reduce the rate at which stress increases (and safety factors decrease) with body mass (McMahon, 1973; McMahon, 1975; Garcia and da Silva, 2004).

Positive allometric scaling of duty factor would reduce strain rate in the long bones of heavier species, and has been identified in a sample of varanid lizards (Clemente et al., 2011). However, duty factor at a given Froude number appears mass-invariant across a broad sample of mammals and birds (Biewener, 1983; Gatesy and Biewener, 1991). Alexander and Jayes (1983) found different sized mammals used equal duty factors at low Froude numbers, while at high Froude numbers noncursorial mammals used larger duty factors than cursorial mammals.

Similarly, unusual asymmetrical gaits lacking a whole-body aerial phase have been reported in some large mammals (Hutchinson et al., 2003; Schmitt et al., 2006), and may assist in reducing vertical oscillations in the center of mass while ambling (Gambaryan, 1976). Yet other large mammals, such as the white rhinoceros, *Ceratotherium simum*, employ a galloping gait while maintaining safety factors in excess of those of other larger quadrupeds (Alexander and Pond, 1992).

The theory of postural modification (Biewener, 1989), in which larger species maintain stress levels by aligning limb segments closer to the line of action of the ground reaction force (GRF) is a means by which mammals can achieve mass-invariant safety factors. By vertically aligning joints more closely to the point of limb attachment, an increasing proportion of total load is born in compression rather than bending. Bone is much stronger in compression than tension (Currey, 2002), and a decrease in tensile stress would cause a reduction in total strain and a subsequent increase in safety factor. Similarly, by increasing the effective mechanical advantage (EMA; the ratio of muscle moment arm to GRF moment arm) of the antigravity muscles, less muscular force is required to oppose GRF, which should again reduce bone loading. Positive allometric scaling of EMA in limbs has been found to characterize a wide range of mammals, spanning from a mouse to a horse (0.1–300 kg in body mass; (Biewener, 1989), and across several species of cercopithecine primates (Polk, 2002). However, changes of posture with body mass may be more complex than originally thought, and in animals larger than 300–500 kg, all options for postural modification may be exhausted (data for EMA scaling in this size range is sparse; but see Ren et al., 2010). Stronger positive allometric scaling of long-bone dimensions may therefore be required to achieve stress similarity in the largest individuals (Christiansen, 1999b; Economos, 1983).

Evidence for "differential scaling" of hind limb dimensions between small and large mammal groups remains equivocal however. Campione and Evans (2012) failed to find any significant differences in femoral length or circumference scaling exponents to body mass between size classes, regardless of whether the boundary was drawn at 20, 50, or 100 kg. Interestingly, postural data from Biewener (1989, 2005) cited above have been reinterpreted as demonstrating two postural groups (crouched, 0.01–1 kg; erect, 1–300 kg) which would suggest two distinct scaling patterns in EMA (Reilly et al., 2007). In this interpretation, large erect mammals experienced a significant increase in EMA with body size, enabling a size-dependent decrease in the relative mass of limb musculature required to maintain their posture. In contrast, small crouched mammals failed to scale EMA significantly with body mass. Limb posture was found to remain relatively constant across the "crouched" size range, with low stresses instead being maintained by relatively increasing limb muscle mass.

Unlike mammals, the sprawling limbs of iguanas and alligators are characterized by decreasing EMA with an increasingly erect posture (Blob and Biewener, 2001), although this is interpreted as being related to torsional loading due to their unusual hindlimb retraction system (Reilly et al., 2005). There are no existing data regarding the scaling of avian EMA across their entire size range (Biewener, 2005), although smaller birds have been found to possess a more crouched posture (calculated as hip height normalized against total segment length) relative to large flightless birds (Gatesy and Biewener, 1991).

A problem common among previous studies of bone scaling is that, in general, they concentrate on a particular measure (such as diameter or second moment of area) as a proxy for bone stress. However, to evaluate biomechanical arguments relating to bone loading and safety factors effectively, we need to consider more than these single measures: bone stress is a function of bone length, curvature, cross-sectional geometry, and angle,

and these can be combined mathematically to evaluate the actual relative stiffness of a particular bone. Previous studies that have addressed the scaling of stress (or proxies for relative strength) to body mass have focused on specific phylogenetic groups (Demes and Jungers, 1993; Rocha-Barbosa and Casinos, 2011). In this study, we calculate the maximum force a bone is capable of withstanding before yield under several static loading regimes, to investigate the scaling of safety factors with body size in a wide range of birds and mammals. We consider the impact of bone robusticity, curvature, and angle on safety factors, and discuss the results in the context of locomotion and peak dynamic forces.

METHODS AND MATERIALS

Skeletal Sample

Data were recorded from the femora and tibiae of 31 species of terrestrial mammals and 29 species of birds, ranging in body mass from 12.5 g (*Sorex araneus*, Common shrew) to 4.03 tons (*Elephas maximus,* Indian elephant). Specimens were selected to include as broad a range of body masses and as many clades as possible (a full list of specimens is included in Table 1). Only skeletally mature individuals were included in the final analyses to avoid any ontogenetic growth allometry. In mammals, skeletal maturity was indicated by fusion of the epiphyses, whereas in birds, it was determined by the loss of surface porosity (Tumarkin-Deratzian et al., 2006) and plumage records when available. Most specimens were sourced from museum collections (National Museums Scotland, Edinburgh; The Manchester Museum and The World Museum, Liverpool), with additional primate CT scans sourced from the Digital Morphology Museum, Kyoto University Primate Research Institute (KUPRI; www.pri.kyoto-u.ac.jp). When an associated body mass for the individual was not available from museum records, values were assigned from the literature (Table 1). External length measurements were taken with digital calipers, with the exception of the largest mammal bones, which were measured with an anthropometer.

Computed Tomography and Image Analysis

CT was carried out on whole bones specimens. Small bird and mammal bones (up to 300 mm in length, 51/60 in this study) were mounted in floral foam (OASIS, Smithers-Oasis UK, Washington, UK) in an array of up to 13 bones, and scanned in the Henry Moseley X-ray Imaging Facility, University of Manchester (X-Tek HMX 225 Custom Bay, Nikon Metrology, Tring, UK). Voxel size ranged between 53 and 119 μm, depending upon maximum bone length. Beam voltage (50–160 kV) and beam current (185–331 μA) were selected to maximize contrast between cortical bone and air. CT data were imported into CT Pro (Nikon Metrology, Tring, UK), the center of rotation determined, noise levels reduced, and the level of beam hardening selected. CT scans comprised between 652 and 2,499 tomographic slices. Data were exported in unsigned 16-bit DICOM format (VG Studio Max v. 2.0, Volume Graphics, Heidelberg, Germany).

Large bird and mammal specimens (N=6) were scanned in a helical CT scanner at the University of Liverpool Small Animal Teaching Hospital (Siemens SOMATOM Volume, Erlangen, Germany). Nominal pixel spacing ranged between 191 and 790 μm voxel^{-1}, beam voltage between 120 and 140 kV and beam current between 100 and 227 μA. CT data were imported into Syngo (Siemens, Erlangen, Germany) for reconstruction with a dedicated kernel (B70s very sharp kernel, Siemens Medical Solutions). A tomographic slice ranged from 1–3 mm in thickness, with scans comprising 173–380 slices in total.

CT data for a small number of primates (N=3) were sourced from the Digital Morphology Museum, KUPRI. Scans were taken of whole carcasses, resulting in pixel spacings of 468–684 μm voxel^{-1}. Femora and tibiae were isolated from primate skeletons (OsiriX 32-bit, v. 3.8), and exported as unsigned 16-bit DICOMs.

As different pixel spacings were used for different-sized specimens, we compared measurements calculated from CT images against those taken manually with calipers to ensure no bias was introduced by imaging small and large bones at varying pixel spacings (with the exception of KUPRI specimens, to which access was not possible). For anteroposterior diameter (d_{AP}), for example, percentage deviation between CT and caliper-derived values was <5%, and no relationship was found between deviation and body mass M_b (kg) of the specimen (deviation N=93.7 log $M_b^{0.62}$, r^2=0.02, P>0.05). Image calibration therefore did not unduly influence our results, and comparisons made between images derived from different machines under different conditions are valid.

Individual bones were cropped from original CT scans consisting of multiple specimens (MATLAB, v. 7.10, Mathworks, Natick, Massachusetts), exported as TIFF files and read into OsiriX. Splint-like fibulae were frequently damaged, unattached, or entirely missing from museum-sourced tibiae and to facilitate comparison these were removed from any specimens where they were present.

Tomographic slices were imported into ImageJ (version 1.46, www.rsbweb.nih.gov/ij) as virtual stacks. The "slice geometry" function of the BoneJ plug-in (version 1.2.4, Doube et al., 2010) for ImageJ was used to calculate internal bone geometric properties from a CT image taken at 50% midshaft length. Orthogonal anteroposterior and mediolateral axes were assigned to each specimen using the "orientation" function of the BoneJ plug-in. Minimum threshold pixel values for bone were defined as 40% of the difference between maximum cortical bone values and minimum values of air within the medullary cavity for each individual specimen. All pixels above the designated minimum threshold were considered as "bone" for the purposes of image analysis. Only *Elephas* was found to possess significant trabecular fill of the medullary cavity but since this still represented a very small fraction of solid bone it was digitally removed and not included in subsequent analysis.

Maximum Force Calculations

Cortical area (CA, mm^2) was calculated as the area of compact bone (defined by threshold values) within a given cross section. Both maximum and minimum values for second moment of area (I_{max} and I_{min}) and values in the anteroposterior and mediolateral direction (I_{AP} and I_{ML}) were calculated directly from the CT images, reflecting bending resistance about said axes (see Fig. 1). Polar moments of area (J, mm^4) were calculated as the sum of

TABLE 1. Specimen list

Binomial name	Common name	Sex	Museum	Accession number	Body mass (kg)
Birds					
Buteo buteo	Common buzzard	U	MM	BB.9009.8	0.875[1]
Haliaeetus albicilla	White-tailed eagle	U	NMS	Z.2000.23	4.795[1]
Accipter nisus	Eurasian sparrowhawk	U	MM	BB.9009.3.1	0.238[1]
Anas crecca	Common teal	U	WML	1982.1081	0.341[1]
Branta leucopsis	Barnacle goose	U	MM	BB.9009.1	1.687[1]
Apteryx haasti	Great spotted kiwi	M	NMS	Z.1913.48	1.900[2]
Uria aalge	Common guillemot	U	MM	BB.9009.5.1	0.993[1]
Fratercula arctica	Atlantic puffin	U	WML	23.7.84.3	0.381[1]
Haematopus ostralegus	Eurasian oystercatcher	U	MM	BB.9009.4.1	0.526[1]
Larus marinus	Great black-backed gull	F	NMS	BL1	0.860*
Columba mayeri	Pink pigeon	U	NMS	PS103.04	0.303[1]
Pezophaps solitaria	Rodrigues solitaire	U	WML	T9598	11.30[3]
Raphus cucullatus	Dodo	U	WML	1981.144	10.20[4]
Gallus sonnerati	Sonnerat's junglefowl	M	NMS	035.47.03	0.963[1]
Lagopus scoticus	Red grouse	F	NMS	035.04.01	0.516[1]
Numida meleagris	Helmeted guinea fowl	U	MM	BB.9009.2.1	1.299[1]
Gavia immer	Great northern diver	F	NMS	Z.1994.36.2	4.100*
Gallinula chloropus	Common moorhen	M	NMS	Z.2004.20.1	0.340[1]
Rallus aquaticus	Water rail	M	NMS	PS 24.2000	0.125*
Ardea cinerea	Grey heron	U	MM	BB.8989.9.1	1.443[1]
Phalacrocorax carbo	Great cormorant	F	NMS	Z.2004.185	1.356*
Phoenicopterus ruber	Rosy flamingo	F	NMS	Z.2000.193.1	2.600*
Diomedea exulans	Wandering albatross	U	NMS	Z.1921.143.163	7.650[1]
Strigops habroptilus	Kakapo	U	NMS	Z.1938.56.1	1.670[1]
Strix aluco	Tawny owl	U	MM	BB.7283.766	0.475[1]
Pygoscelis papua ellsworthi	Gentoo penguin	M	NMS	Z.2007.66	4.04*
Struthio camelus	Ostrich	U	NMS	Z.1930.15.1	83.50[1]
Casuarius unappendiculatus	Northern cassowary	F	NMS	Z.1995.119.1	58.00[5]
Tinamus solitarius	Solitary tinamou	F	NMS	PS 276/04	1.550[1]
Mammals					
Giraffa camelopardalis	Giraffe	M	NMS	Z.2001.148.3	1192[6]
Acinonyx jubatus	Cheetah	M	NMS	GH353.09	50.17[7]
Nasua nasua	Ring-tailed coati	U	MM	A.2305.9	3.60[7]
Mustela putorius	European polecat	M	NMS	Z.2000.307.4	1.11[7]
Vulpes cana	Blanford's fox	M	NMS	Z.2004.46.13	1.630*
Pteropus rodricensis	Rodrigues fruit bat	M	NMS	Z.2003.144.4	0.305*
Petaurus breviceps	Sugar glider	M	NMS	Z.2000.175.2	0.096*
Erinaceus europaeus	European hedgehog	U	WML	1988.226	0.682[7]
Procavia capensis	Rock hyrax	M	NMS	Z.2009.076	3.14[7]
Lepus europaeus	European hare	U	WML	1982.706	2.85[7]
Ochotona dauurica	Daurian pika	U	NMS	Pika 3.	0.128[7]
Oryctolagus cuniculus	European rabbit	U	WML	1988.22w	1.74[7]
Ornithorhynchus anatinus	Platypus	U	WML	28.12.65.1	1.501[7]
Tachyglossus aculeatus	Short-beaked echidna	M	NMS	Z.2009.81	6.80*
Callicebus cupreus	Red titi	M	NMS	Z.2004.171	1.210*
Callimico goeldii	Goeldi's monkey	M	NMS	Z.2001.61.4	0.468*
Cheirogaleus medius	Fat-tailed dwarf lemur	U	NMS	R150/97	0.231*
Chlorocebus aethiops	Grivet monkey	M	KUPRI	PRI-CA14	5.50[8]
Galago senegalensis	Senegal bushbaby	F	NMS	Z.2002.94.2	0.220*
Gorilla beringei	Eastern lowland gorilla	M	NMS	Z.2001.156	139.5[8]
Hylobates lar	Lar gibbon	F	KUPRI	PRI-9265	5.60[8]
Pan paniscus	Bonobo	M	W.Sellers	-	39.00[8]
Pan troglodytes	Common chimpanze	F	NMS	Z.2009.120	39.50[8]
Pithecia pithecia	White-faced saki	F	NMS	Z.2003.42.1	3.800*
Pongo pygmaeus	Bornean orangutan	F	W.Sellers	-	37.00[8]
Saimiri sciureus	Squirrel monkey	F	KUPRI	PRI-Ss116	0.774[8]
Elephas maximus	Indian elephant	F	NMS	Z.2001.147	4025*
Cavia aperea	Brazilian guinea pig	F	NMS	Z.2004.149.3	0.334*
Fukomys anselli	Ansell's mole rat	F	NMS	Z.2009.124.2	0.0225*
Sciurus vulgaris	Red squirrel	M	NMS	Z.2003.107.5	0.371*
Sorex araneus	Common shrew	F	NMS	Z.2003.11	0.0124*

MM, Manchester Museum; NMS, National Museum of Scotland, Edinburgh; WML, World Museum, Liverpool; KUPRI, Kyoto Primate Research Institute, Kyoto. Associated body mass (kg) denoted with asterisk. Assigned body masses taken from following sources: [1] (Dunning, 1993), [2] (Davies, 2003), [3] (Livezey, 1993), [4] (Angst et al., 2011), [5] (Davies, 2002), [6] (Smithers, 1983), [7] (Silva and Downing, 1995), [8] (Wisconsin National Primate Research Centre, 2011).

two orthogonal measures of second moment of area for each cross section ($I_{max}+I_{min}$) (Boresi and Schmidt, 2002), and reflect resistance to torsion.

When calculating the stress acting within a bone, a value for body mass (recorded or estimated) must be included in the form of force (F, the multiple of mass and gravitational acceleration). For example, the compressive stress (σ_c) acting on a bone loaded in pure axial compression is typically calculated as:

$$\sigma_c = \frac{F}{CA} \quad (1)$$

where CA is the cross sectional area (m^2). However, if predicted stress values were subsequently scaled against body mass, the mass variable would be present on both sides of the equation and the correlation would be invalid. We therefore rearrange commonly used equations for stress to solve for force, substituting in geometric parameters and values for yield stress. As such, we calculate the maximum force a bone is capable of withstanding before yield for the given loading condition. Maximum compressive force is therefore:

$$F_c = \sigma_c CA \quad (2)$$

This equation ignores the potential effects of induced bending as a result of compressive forces acting longitudinally around curvature of the shaft. Considerable curvature of hind limb bones has been identified in both mammals (Bertram and Biewener, 1988) and birds (Cubo et al., 1999), and any potential scaling effects must be incorporated into final estimates of maximum force. The moment arm of the axial load exerting a bending moment about the midshaft was calculated as the orthogonal distance taken from a chord joining proximal and distal epiphyses, to the centroid at midshaft (Biewener, 1983) in a custom MATLAB script. The angle of curvature (ξ) was then calculated at the proximal epiphysis, as the intersection between the proximal-distal chord and the centroid-proximal chord (see Fig. 2). The combined effect of compressive and induced bending forces were calculated as:

$$F_c = \frac{\sigma_c I_{AP} CA}{I_{AP} cos\xi + CA(0.5l) r_{AP} sin\xi} \quad (3)$$

where l is the total element length (m), and r_{AP} is the distance (m) from the section centroid to the periosteal contour along the anteroposterior axis, and I_{AP} is the second moment of area in the anteroposterior direction (m^4) (rearranged from Alexander, 1974).

Maximum bending force (F_b) in the AP direction is estimated as:

$$F_b = \frac{\sigma_b I_{AP}}{(0.5l) r_{AP}} \quad (4)$$

assuming the bone is held horizontally and clamped at midshaft to act as a cantilever (rearranged from Alexander, 1974). Again, this ignores any potential effects of curvature on total force values. Instead, maximum resistible force when bending a curved bone in the plane of initial curvature was estimated by incorporating the value k into eq. 4 as:

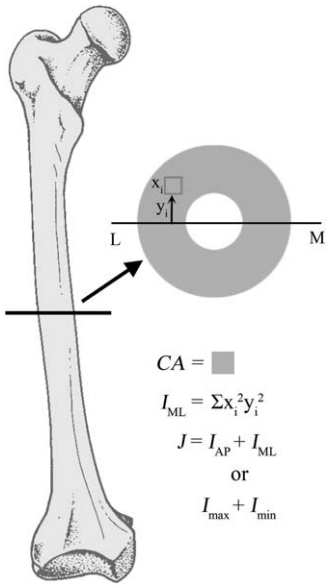

Fig. 1. Calculation of cortical area (CA), second moments of area (I), and polar moment of area (J). I is calculated for a cross section as the sum of the area of every "pixel" multiplied by the squared distance of said pixel from the axis of interest.

$$F_b = \frac{\sigma_b I_{AP}}{(0.5l) r_{AP} k} \quad (5)$$

where

$$k = 1 + 0.5 \frac{I_{AP}}{d_{ML} r_{AP}^2} \left[\frac{1}{R - r_{AP}} + \frac{1}{R} \right] \quad (6)$$

when d_{ML} is the diameter (m) in the mediolateral direction, and R is the radius of curvature (m) calculated according to the intersecting chords theorem (Roark, 1965) (see Fig. 2).

The maximum torsional force (F_t) a bone is capable of resisting before yield was calculated as:

$$F_t = \frac{\sigma_t J}{(l_{alt}) r_{max}} \quad (7)$$

where the torsional moment arm l_{alt} (m) is considered to be proportional to the length of the alternative bone element (femur length in the case of a twisting tibia, and *vice versa*) upon which the force due to the body mass acts as a lever (Clemente et al., 2011). Diagrams of the three load cases considered above are shown in Fig. 3. Maximum section radius r_{max} (m) was used in the calculation of torsional moment, and resulting torsional forces therefore reflect maximum possible values. The calculation of F_t in this manner is likely to be very approximate, as the application of polar moments of area rests upon an assumption of thin-walled hollow tubes with axial symmetry (i.e., a uniform cylindrical cross-sectional shape) (Roark, 1965), a situation frequently invalidated in vertebrate long bones (Brassey et al., 2013). Furthermore, the possibility of a hindlimb element being loaded in pure torsion *in vivo* is extremely unlikely, and

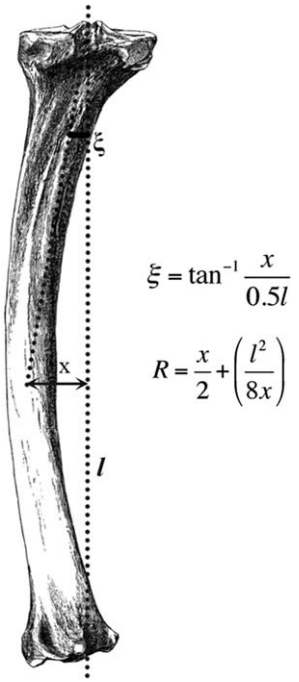

Fig. 2. Calculation of curvature angle (ξ) and radius of curvature (*R*). *l*, total chord length; *x*, orthogonal distance between centroid at midshaft and chord connecting proximal and distal epiphyses.

therefore calculated torsional loads may be unreasonably high. With these caveats in mind, torsional force is included in the present study to facilitate comparison with better-understood compressive and bending force.

The evolutionary history of vertebrates has been broadly characterized by conservation of material properties (Erickson et al., 2002), and locomotory challenges have been overcome predominantly by changes in bone size and shape. The potential for high intraspecific ontogenetic variation in Young's modulus (*E*) must be recognized (*Ursus maritimus* femur under torsion at 3 months, E=6.7 GPa; at 6 months, E=11.2 GPa; (Currey, 2002)). However, osteologically mature long-bone material properties are relatively restricted across broad phylogenetic groups, particularly when viewed in context of the immense diversity in morphology and body size characterizing the same groups. Young's modulus ranges between 10 and 20 GPa in intact avian long bones (Cubo and Casinos, 2000), and 15–25 GPa in mammal long bones (Zioupos et al., 2000; Erickson et al., 2002).

Cortical bone is weaker in tension than compression, and values of σ_c=180 MPa and σ_b=128 MPa for yield stress were used in the above equations (Cezayirlioglu et al., 1985). Under torsion, cortical bone is weaker still, and a value of 53 MPa for σ_t was used to calculate maximum torsional force (Cezayirlioglu et al., 1985).

The maximum body mass (M_b^{max}) a leg bone is capable of supporting under a given loading condition was calculated as:

$$M_b^{max} = \frac{F}{ga} \quad (8)$$

where g is gravitational acceleration (9.81 m s^{-2}), and a is a fraction reflecting the proportion of body mass supported by the hindlimbs (Alexander and Pond, 1992). In the case of birds, a=1. The broad phylogenetic diversity of the mammalian sample in question does not permit species-specific values of a to be assigned, and a value of 0.4 was used for mammals throughout. Safety factors were then calculated as the ratio of maximum body mass to given body mass:

$$SF = \frac{M_b^{max}}{M_b} \quad (9)$$

The relationship between maximum combined compressive and bending force (F_{cb}), and limb orientation was described as:

$$F_{cb} = \frac{\sigma_b I_{AP} CA}{(sin\theta I_{AP} cos\xi) + CA(0.5l) r_{AP}(sin\theta sin\xi + cos\theta)} \quad (10)$$

where θ is the angle from the horizontal (Alexander, 1974). Values of combined force (F_{cb}) were calculated for θ between 0 and 90 degree, and curves describing the relationship between the resulting safety factors and bone angle plotted. The maximum angle from vertical (θ_{max}) at which each bone may be held for a given SF was given as the intersection of each species-specific curve with horizontal lines representing various factors of safety (12–20). These values are considerably larger than the typical safety factors calculated from peak dynamic stress (Biewener, 1982; Rubin and Lanyon, 1982), and reflect the static nature of this model. Values for θ_{max} were plotted against body mass to investigate scaling of hindlimb posture with body size.

Calculation of Scaling Exponents

Slopes were fitted by means of standardized major axis (SMA), a type II regression, in the "smatr" package (Warton et al., 2006) of statistical software "R" (www.cran.r-project.org). SMA is an appropriate regression model to use when error is introduced in both *X* and *Y* variables (particularly when the error rate of the *X* variable is over one-third of that on the *Y;* (McArdle, 1988) and when the values being compared are of fundamentally different types (e.g., mass and distance). In this instance, error was introduced on the *X* axes through the inclusion of literature values for some body masses. However, when correlation coefficients do not approach 1, the potential for strong slope inflation relative to ordinary least squares (OLS) slopes must be taken into account (Warton et al., 2006). When exploring the relationship between bone length to radius of curvature, and θ_{max} to body mass (Table 4, Fig. 10), characterized by low r^2 values, Type-I OLS regressions were therefore preferred.

In addition to conventional statistical methods, we applied a phylogenetically based model to account for evolutionary relationships and statistical nonindependence of residuals. We constructed a composite phylogeny using Mesquite ver. 2.75 (http://mesquiteproject.org), with tree topology and branch lengths based on existing published phylogenies (see Figs. 4 and 5). Both dependent and independent variables were log transformed. A phylogenetic variance-covariance matrix was exported from Mesquite (export PDDIST function), and the MATLAB program "Regressionv2.m" (Lavin et al., 2008) used

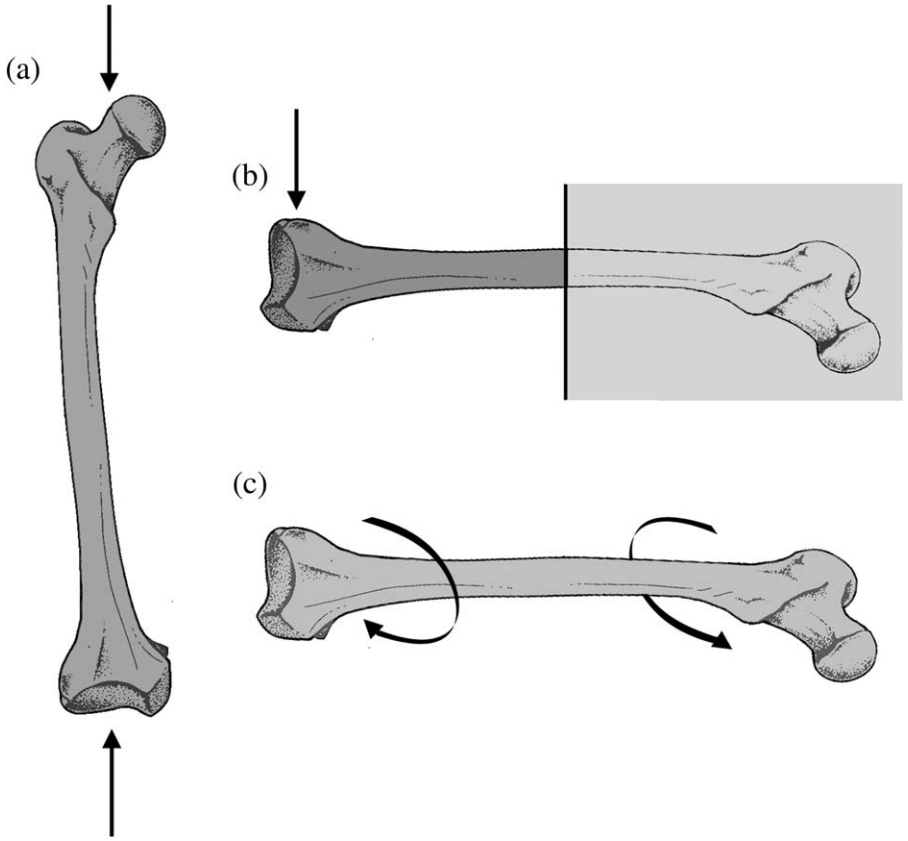

Fig. 3. Sketched of load cases considered. (**a**) axial compression; (**b**) clamped at midshaft and loaded under bending; (**c**) torsion.

to implement nonphylogenetic and phylogenetic regressions. Unlike ordinary least squared (OLS), phylogenetic generalized least squares (PGLS) assumes residuals are correlated, and are given by a Brownian motion model of evolution inferring a relatively strong phylogenetic signal. To estimate the strength of the phylogenetic signal in residual variation, correlation between residuals was also modeled as an Ornstein-Uhlenbeck evolutionary process (RegOU) which is often used to model the wandering motion of a population back and forth around an optimum peak (Felsenstein, 1988; Lavin et al., 2008). To compare the goodness of fit of the three models (nonphylogenetic, PGLS and RegOU), the Akaike Information Criterion (AIC) is included in Table 3 (smaller value implies better fit of model to data). As a general rule of thumb, models with an AIC of <2 units greater than the minimum AIC value are also said to have considerable support, while a difference of 4–7 units suggests considerably less support (Gartner et al., 2010). The optimal Ornstein–Uhlenbeck transformation parameter (d) was also estimated using the Regressionv2.m program. When $d=1$, the PGLS model is said to best fit the data, while a d value of 0 suggests the OLS model is the best fit (Lavin et al., 2008).

A one-sample test of slope was used to determine if SMA slope values differed from a specified scaling exponent, by testing for correlation between the residual and fitted axis scores (Warton et al., 2006). Differences between SMA slopes were tested for using a Bartlett-corrected likelihood ratio (lr) test in smatr, which is analogous to an ANCOVA on OLS slopes. Mean radius of curvature and safety factor values were compared between phylogenetic groups ("mammal" vs. "bird") and between hindlimb elements ("femur" vs. "tibia") using a two-way ANOVA with post hoc Tukey HSD test implemented in R.

RESULTS

Scaling of Cross-sectional Properties

Scaling exponents for external dimensions and cross-sectional properties against body mass are provided in Tables 2 and 3, including both untransformed and phylogenetically corrected values. With the exception of avian tibiotarsal length and d_{AP}, nonphylogenetic OLS models provided better fits to the data (i.e., had a more negative AIC value) as compared to the phylogenetic PGLS and RegOU models (Table 3). However, RegOU models typically had AIC values ≤ 2 units greater than the comparable OLS model, suggesting this phylogenetic model also had considerable support. Values for the optimal Ornstein-Uhlenbeck transformation parameter (d) were typically much closer to zero than one, suggesting that the OLS model provided a better fit to the data that the PGLS (Lavin et al., 2008). For this reason, the chosen sample was not considered to be biasing the regressions,

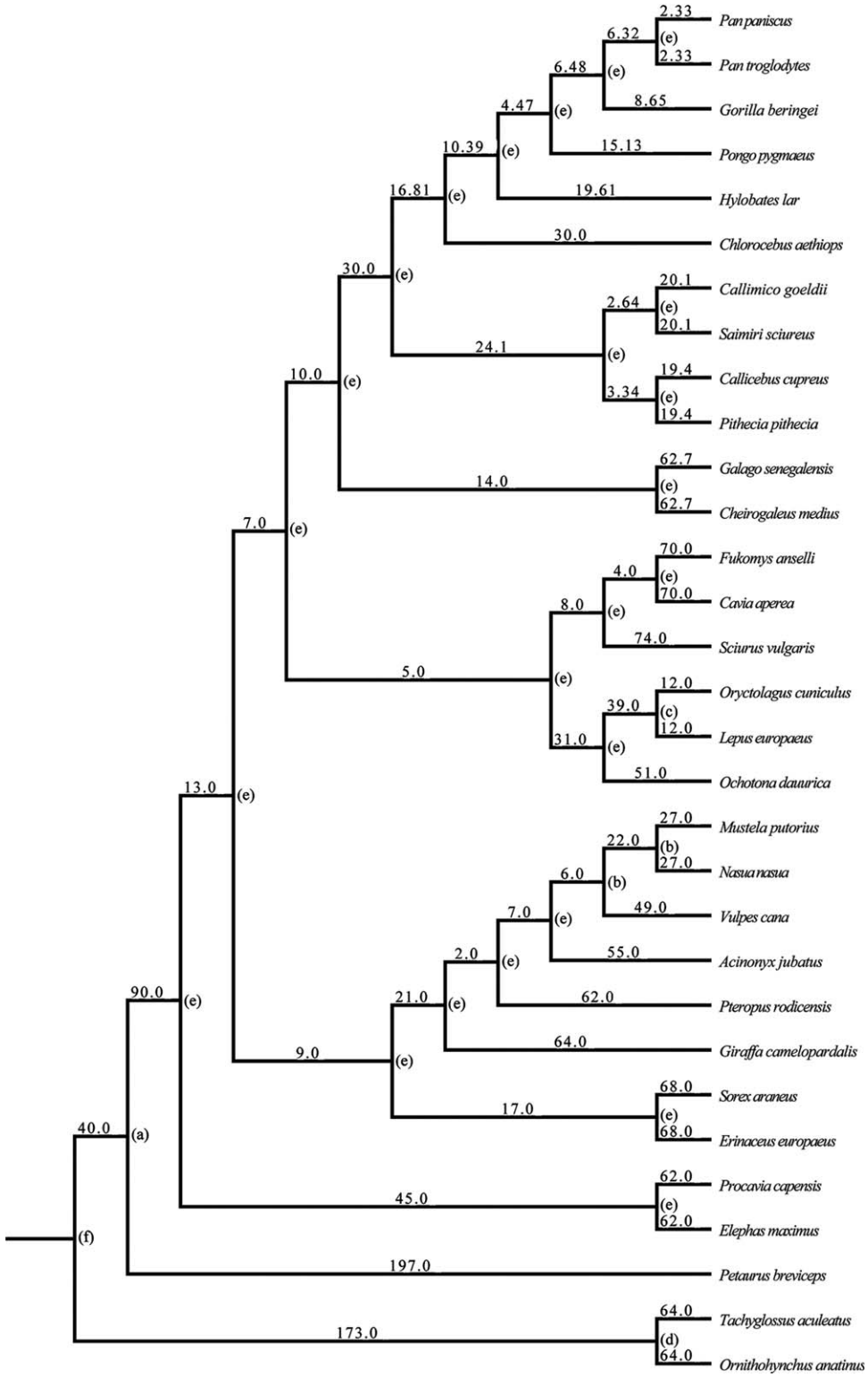

Fig. 4. Mammal consensus tree. Branch lengths given in millions of years (Mya). Tree topology based upon class-level genomic sequence study (Prasad and Allard, 2008), and several order-level molecular studies: Carnivora (Agnarsson et al., 2010); Rodentia (Blanga-Kanfi et al., 2009); Artiodactyla (Decker et al., 2009); Afrotheria (Seiffert, 2007); Primates (Arnold et al., 2010). Branch lengths taken from the following sources: [a] (Beck, 2008); [b] (Eizirik et al., 2010); [c] (Matthee et al., 2004); [d] (Rowe et al., 2008); [e] (Springer et al., 2003); [f] (Woodburne et al., 2003).

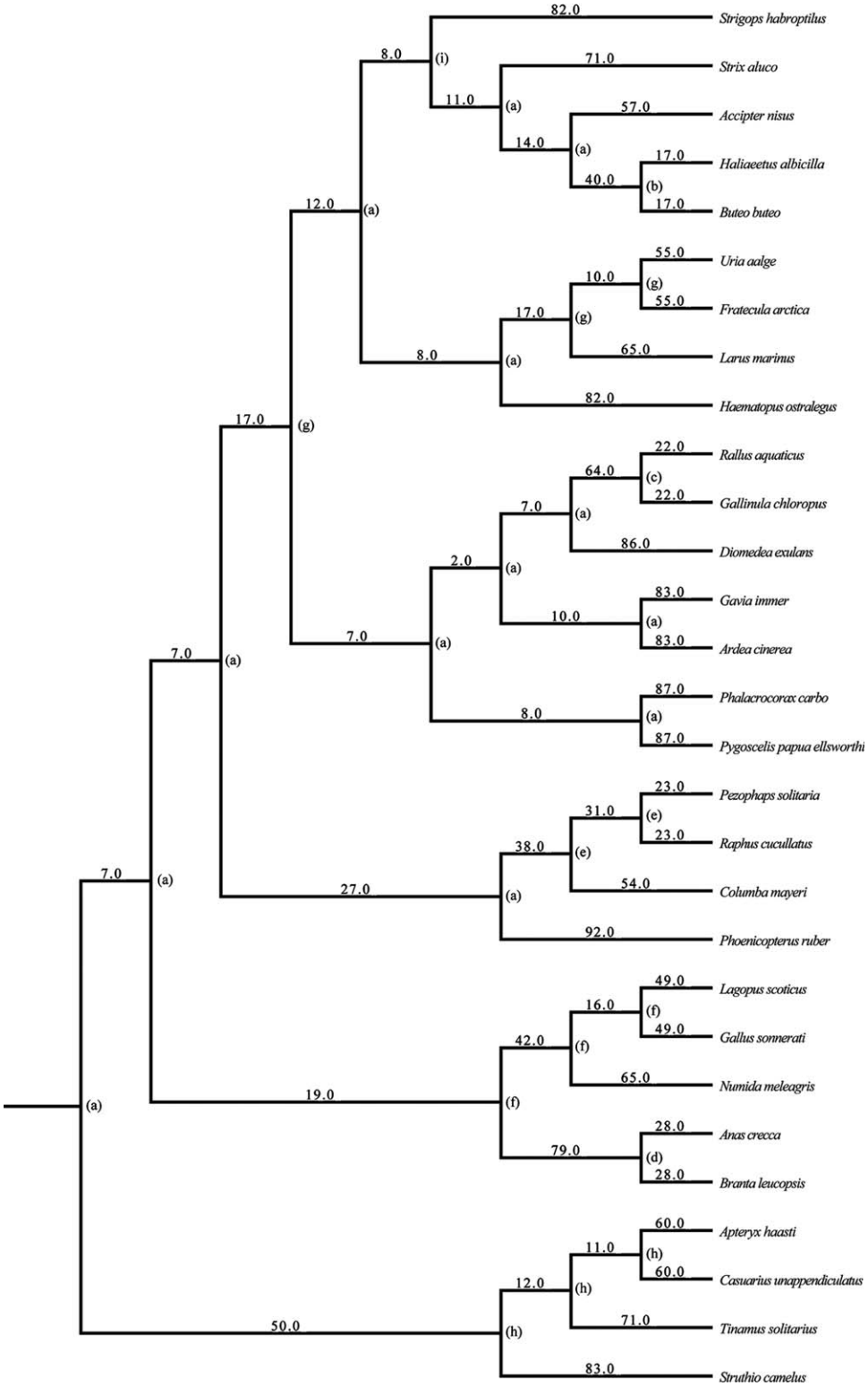

Fig. 5. Bird consensus tree. Branch lengths given in millions of years (Mya). Tree topology based upon class-level molecular study (Hackett et al. 2008) and an additional ratite genome study (Phillips et al., 2010). Branch lengths taken from following sources: [a] (Brown et al., 2008); [b] (do Amaral et al., 2009); [c] (Fain et al., 2007); [d] (Gonzalez et al., 2009); [e] (Pereira et al., 2007); [f] (Pereira and Baker, 2006); [g] (Pereira and Baker, 2008); [h] (Phillips et al., 2010); [i] (Wright et al., 2008).

TABLE 2. SMA regression of long-bone length and cross-sectional properties against body mass

	n	a	b	95% CI	r^2	P (isometry)
Mammal femur						
l	31	−1.18	**0.35**	0.31–0.40	0.89	0.26
d_{AP}	31	0.74	**0.37**	0.35–0.40	0.96	0.002**
CA	31	−4.77	**0.74**	0.68–0.80	0.96	0.01*
I_{AP}	31	−10.32	**1.46**	1.36–1.56	0.97	0.01*
J	31	−10.05	**1.46**	1.37–1.57	0.97	0.007**
Mammal tibia						
l	31	−1.16	**0.31**	0.28–0.35	0.90	0.33
d_{AP}	31	0.69	**0.39**	0.34–0.43	0.91	0.01*
CA	31	−4.89	**0.73**	0.67–0.80	0.94	0.03*
I_{AP}	31	−10.72	**1.44**	1.33–1.56	0.95	0.06
J	31	−10.37	**1.47**	1.34–1.61	0.94	0.03*
Bird femur						
l	29	−1.21	**0.34**	0.29–0.4	0.83	0.80
d_{AP}	29	0.79	**0.42**	0.38–0.47	0.92	<0.001***
CA	29	−4.8	**0.82**	0.72–0.93	0.90	0.001**
I_{AP}	29	−10.3	**1.67**	1.48–1.91	0.90	<0.001***
J	29	−9.85	**1.68**	1.49–1.88	0.91	<0.001***
Bird tibia						
l	29	−0.98	**0.38**	0.32–0.44	0.85	0.10
d_{AP}	29	0.72	**0.39**	0.36–0.43	0.95	<0.001***
CA	29	−4.86	**0.82**	0.75–0.89	0.95	<0.001***
I_{AP}	29	−10.38	**1.64**	1.50–1.79	0.95	<0.001***
J	29	−10.12	**1.64**	1.50–1.79	0.95	<0.001***

Regression statistics in the form $\log Y = a \log M_b^b$, where Y is an osteological parameter and M_b is body mass in kilograms. Slopes were fitted to the data by means of Model II SMA regression. Scaling exponents are given in bold. Asterisks denote level of significance (likelihood ratio test) between calculated slope and those predicted by isometry: *$P<0.05$; **$P<0.01$; ***$P<0.001$. 95% confidence intervals (CI) and r^2 values are provided.

and only uncorrected Type I and II models are discussed in further detail.

To ensure the inclusion of fliers/gliders (*Pteropus rodricensis, Petaurus breviceps*), saltators (*Lepus europaeus, Oryctolagus cuniculus*), and aquatic species (*Ornithorhynchus anatinus*) was not heavily biasing mammalian regressions, models were re-run while excluding these specialist species. For regressions of cross-sectional properties against body mass (Table 2), original slope values and re-run slope values were not significantly different from one another (lr=0.23, $P=0.64$). Likewise, for regressions of estimated maximum force against body mass (Table 5), no difference was found in slope values upon excluding specialist species (lr=0.36, $P=0.55$). All slopes that were originally found to be significant remained so, correlation coefficients improved slightly, and interpretation of results was not affected.

We also investigated the effects of removing primates from the mammalian sample. No difference was found between slopes including and excluding primates, when regressing cross-sectional properties against body mass (lr=0.77, $P=0.38$), or regressing estimated maximum force against body mass (lr=0.44, $P=0.51$). Primate quadrupedalism is characterized as hindlimb dominated (Demes et al., 1994). We therefore investigated the effects of assigning primates a hindlimb loading ratio of $a=0.6$, while holding the remainder of the mammals at 0.4. For regressions of maximum angle (θ_{max}) against body mass (Fig. 10), no difference was found between original slopes and those with primate-specific hindlimb loading ratios (lr=0.32, $P=0.57$). Despite containing several different locomotor groups, no attempt was made to subdivide the avian sample, as results elsewhere have suggested scaling exponents are not significantly different among functional groups (Doube et al., 2012).

Length did not scale differently from isometry across several orders of magnitude in body size of mammals (r=0.21, $P=0.26$) and birds (r=0.31, $P=0.10$), with all confidence intervals including the value of 0.33 predicted by geometric similarity (Table 2). With the exception of I_{AP} of the mammalian tibia, all other dimensions scale more strongly than isometry (r=0.39, $P<0.03$ in mammals; r=0.57, $P\leq0.001$ in birds). Cross-sectional properties scale with greater positive allometry in avian hindlimbs than those of mammals (Table 2), although this difference is significant only for scaling exponents of femoral and tibial I_{AP} (lr=4.05, $P<0.05$) and femoral J (lr=3.93, $P<0.05$).

Scaling of Long-Bone Curvature

The scaling exponents of radius of curvature (R) against bone length are given in Table 4. As radius of curvature is a linear measurement, geometric similarity would predict $R \propto l^1$. In both the mammalian tibia and avian femur, there is a significant relationship between R and length ($r^2>0.46$, $P<0.001$), with both exponents' confidence intervals including 1. The relationship between curvature and bone length in the mammal femur is weak but significant ($r^2=0.15$, $P=0.02$), and the confidence intervals of the slope (0.04–0.88) exclude isometry. For a given body mass, the avian femur is the most curved (smallest R), yet scales R the fastest with length ($R \propto l^{0.94}$) (Fig. 6). In contrast, the avian tibiotarsus is the least curved element investigated, and fails to scale R significantly with body mass ($r^2=0.07$, $P=0.09$).

Applying a two-way ANOVA, the "phylogeny" variable (mammals vs. birds) has a significant effect on mean R (df=116, $F=5.91$, $P<0.02$). A post hoc Tukey HSD test indicates mean R is significantly higher in the avian tibiotarsus than the mammal tibia (df=116, $P<0.001$), while there is no significant difference between bird and mammal femora. The "element" variable (femur vs. tibia) in a two-way ANOVA is significant (df=116, $F=10.7$, $P<0.001$), with a pairwise comparison of means indicating a significant difference between R values in the avian stylopodium and zeugopodium (df=116, $P<0.001$), yet no such difference is present in the mammal hindlimb.

Consequences of Bone Curvature and Robusticity on Maximum Force Scaling

The scaling exponents of maximum force a bone is able to withstand before yielding against body mass under various loading regimes are given in Table 5. All slopes are highly significant ($r^2>0.83$, $P<0.001$). If force were found to scale with body mass as $F \propto M_b^1$, constant safety factors would be achieved. Negative allometry implies safety factors are decreasing with size, while positive allometry implies increasing safety factors with body mass. For all loading regimes considered, the mammalian femur and tibia and avian tibiotarsus scale force with negative allometry, with 95% confidence intervals

TABLE 3. OLS and phylogenetically based regressions of long-bone length and cross-sectional properties against body mass

	OLS					PGLS					RegOU				
	b	±95%	r^2	AIC	ln ML	*b*	±95%	r^2	AIC	ln ML	±95%	*b*	r^2	AIC	ln ML	*d*
Mammal femur																
l	**0.33**	0.045	0.89	−27.3	16.7	**0.32**	0.030	0.92	−0.23	15.0	**0.32**	0.035	0.91	−26.5	15.8	0.49
d_{AP}	**0.37**	0.025	0.96	−57.5	31.8	**0.36**	0.025	0.97	−47.0	26.5	**0.36**	0.025	0.96	−56.6	32.3	0.12
CA	**0.72**	0.055	0.96	−9.58	7.79	**0.71**	0.050	0.96	3.27	1.37	**0.72**	0.055	0.96	−8.87	8.43	0.08
I_{AP}	**1.43**	0.095	0.97	24.1	−9.07	**1.42**	0.105	0.96	47.4	−20.7	**1.43**	0.090	0.97	25.4	−8.68	0.06
J	**1.44**	0.090	0.97	22.7	−8.35	**1.42**	0.090	0.97	41.5	−17.7	**1.44**	0.090	0.97	23.7	−7.87	0.06
Mammal tibia																
l	**0.30**	0.035	0.91	−40.5	23.3	**0.30**	0.035	0.90	−19.2	12.6	**0.30**	0.035	0.91	−38.5	23.3	0.02
d_{AP}	**0.37**	0.040	0.92	−29.5	17.8	**0.36**	0.035	0.93	−19.6	12.8	**0.37**	0.035	0.92	−28.1	18.1	0.19
CA	**0.71**	0.055	0.95	−6.17	6.09	**0.72**	0.055	0.96	7.00	0.50	**0.71**	0.055	0.95	−4.75	6.38	0.17
I_{AP}	**1.41**	0.110	0.96	30.8	−12.4	**1.46**	0.100	0.96	48.4	−21.2	**1.41**	0.100	0.96	32.5	−12.3	0.14
J	**1.43**	0.115	0.95	37.0	−15.5	**1.46**	0.110	0.96	51.8	−22.9	**1.43**	0.110	0.95	38.6	−15.3	0.16
Bird femur																
l	**0.31**	0.055	0.83	−49.8	27.9	**0.30**	0.055	0.82	−46.1	26.0	**0.31**	0.050	0.83	−49.1	28.6	0.26
d_{AP}	**0.41**	0.045	0.92	−57.9	31.9	**0.42**	0.060	0.88	−41.9	23.9	**0.41**	0.040	0.92	−55.9	31.9	0.10
CA	**0.78**	0.090	0.90	−14.9	10.5	**0.80**	0.115	0.87	−0.93	3.46	**0.78**	0.095	0.90	−12.9	10.4	0.10
I_{AP}	**1.60**	0.195	0.90	28.3	−11.1	**1.65**	0.245	0.86	43.1	−18.5	**1.60**	0.190	0.90	30.3	−11.1	0.11
J	**1.60**	0.185	0.91	23.3	−8.63	**1.65**	0.235	0.88	38.6	−16.3	**1.60**	0.180	0.91	25.3	−8.64	0.10
Bird tibia																
l	**0.35**	0.050	0.85	−47.7	26.8	**0.33**	0.050	0.86	−49.5	27.8	**0.33**	0.045	0.86	−47.9	27.9	1.05
d_{AP}	**0.38**	0.030	0.95	−78.3	42.1	**0.38**	0.040	0.93	−62.7	34.3	**0.38**	0.030	0.95	−79.3	42.2	0.10
CA	**0.80**	0.065	0.95	−33.0	19.5	**0.79**	0.085	0.93	−23.0	14.5	**0.80**	0.070	0.95	−31.0	19.5	0.10
I_{AP}	**1.60**	0.135	0.95	5.45	0.27	**1.61**	0.205	0.92	25.2	−9.61	**1.60**	0.135	0.95	7.45	0.27	0.11
J	**1.58**	0.125	0.95	2.19	1.90	**1.58**	0.185	0.92	21.2	−7.6	**1.58**	0.130	0.95	4.19	1.90	0.08

OLS, ordinary least squares; PGLS, phylogenetically generalized least squares; RegOU, phylogenetic regression with Ornstein-Uhlenbeck process; AIC, Akaike Information Criterion; ln ML, natural log maximum likelihood; *d*, restricted maximum likelihood estimate of the Ornstein-Uhlenbeck transformation parameter; ±95%, 95% confidence intervals of the slope value. Scaling exponents are given in bold.

TABLE 4. Allometry of radius of curvature against bone length in mammal and bird hindlimbs

	OLS regression results				
	A	*b*	95% CI	r^2	*P*
Mammal femur	1.74	**0.46**	0.04–0.88	0.15	0.02*
Mammal tibia	0.88	**0.88**	0.52–1.23	0.46	0.001**
Bird femur	0.43	**0.94**	0.63–1.25	0.59	0.001**
Bird tibia	2.14	**0.53**	−0.25 to 1.31	0.07	0.09
Two-way ANOVA					
	F	*p*			
"Phylogeny"	5.91	0.017*			
"Element"	10.69	0.001**			
Interaction	14.06	<0.001***			
Post hoc Tukey HSD test					
	P				
MF:MT	0.99				
BF:BT	<0.001***				
MF:BF	0.79				
MT:BT	<0.001***				
MF:BT	<0.001***				
MT:BF	0.90				

The effect of "phylogeny" (mammal vs. bird) and skeletal "element" (femur vs. tibia) on mean radius of curvature was tested in a two-way ANOVA. A post hoc Tukey HSD test of multiple means indicates pairwise comparisons that are significantly different ($P<0.05$). MF, mammal femur; MT, mammal tibia; BF, bird femur; BT, bird tibiotarsus. A type-I OLS regression was favored due to low correlation coefficients. Scaling exponents are given in bold.

excluding 1 (Table 5, Fig. 7). In the avian femur, force scales with negative allometry under most loading conditions, yet isometry cannot be rejected (confidence intervals include 1) and constant safety factors may be achieved. For each loading regime, a likelihood ratio test for common slopes was applied (Table 6). Scaling exponents were significantly different between groups under each loading condition (lr>8.70, $P<0.03$).

In the case of estimating F_c, incorporating curvature into the equation has the effect of decreasing intercept and slope values in both the mammal femur and tibia, and the avian tibiotarsus (Table 5). In contrast, the scaling exponent of $F_c \propto M_b$ in the avian femur is increased when applying eq. 3. Incorporating curvature into estimates of F_b has very little effect on intercept and slope values. In the avian femur (the most curved element investigated), the ratio of radius of curvature to midshaft radius (R/r) was >50. Such high R/r values result in k values very little above 1 (mean k in avian femur=1.01), and thus contributes very little to the calculation of F_b.

Average safety factors calculated under each loading regime are reported in Table 7. Applying a two-way ANOVA, the phylogeny variable has a highly significant effect on mean SF across loading conditions (df=116, $F>10.5$, $P<0.002$). A post hoc Tukey HSD test indicates mean safety factors are significantly higher in the mammalian femur than in the avian equivalent, while no such relationship exists between the mammal tibia-avian tibiotarsus. The element variable in a two-way ANOVA is also significant for compression and bending loading regimes (df=116, $F > 3.92$, $P<0.05$), with a pairwise comparison of means indicating safety factors are significantly lower in the mammalian zeugopodium than stylopodium ($P=0.05$).

It must be reiterated that the above safety factor values are calculated using static loading models and assume 40% of total body mass is borne through the hindlimbs in the case of mammals, as reported elsewhere (Alexander, 1989; Christiansen, 1998). When testing for the effect of phylogeny on mean safety factors, this hindlimb loading coefficient is incorporated to ensure that we are comparing like for like between bipedal birds and quadrupedal mammals.

Scaling of Limb Orientation

Species-specific safety factor curves (Figs. 8 and 9) indicate a relationship between SF and posture, in which safety factors increase as bones are held close to vertical. When a horizontal line is drawn on these graphs, intersections with SF curves represent the angle respective bones must be held at to achieve a common safety factor. As safety factors are generally lower in birds, it is possible to find a suitable value of SF that may be used to compare almost all species. However, in mammals the minimum safety factor of some species is greater than the maximum safety factor of others. Therefore, a safety factor of 15 was chosen to encompass most of the bird and mammal species. The species excluded by this safety factor (such as the common shrew, mole rat, and pika) all operate at very low bone stresses and postural angle is therefore irrelevant. Plotting θ_{max} against body mass for a safety factor of 15 (Fig. 10) gives a significant positive relationship in the case of mammal hindlimb bones, and avian tibiotarsii ($P<0.01$). For all values of safety factors considered here, there is no relationship between θ_{max} and body mass in the avian femur ($P>0.05$).

DISCUSSION

With the exception of measures of length and curvature, bird and mammal hindlimb bones do not conform to isometry. In addition, despite strong positive allometry of cross-sectional geometric properties, maximum force continues to scale with negative isometry against body mass (Table 5, Fig. 7), demonstrating the allometric scaling of geometry is insufficient on its own to maintain uniform safety factors. The avian femur is shown to behave differently, scaling force to body mass close to isometry and potentially maintaining constant safety factors across a large size range.

Mean safety factors for static compressive loading are universally high (Figs. 8 and 9, Table 7), reaffirming the notion that limb bones do not fail under static compression alone. Incorporating curvature into equations for compression results in large decreases in estimated maximum F_c, yet still does not put bones in danger of actually failing under compressive loading. If curved bones under compression are assumed to fail in tension (due to induced bending), then incorporating the lower value of σ_b into eq. 3 would result in a further decrease in compressive safety factors.

The low correlation coefficient between curvature and length found in the mammal femur ($r^2=0.15$) is similar to those identified in previous studies (Biewener, 1983; Bertram and Biewener, 1992), in which the mammal femur was found not to scale curvature with body mass. In contrast to the above studies however, we found mammal femur R to scale below isometry (i.e., larger individuals have more curved bones), with a P value indicating this result is unlikely to have occurred by chance ($P<0.02$). However, the low correlation coefficient suggests the majority of variation in femoral curvature is due to a factor other than length. As suggested elsewhere, this may reflect a more complex muscle attachment system in the proximal limb (Bertram and Biewener, 1992), or the need to achieve a higher level of strain to promote tissue remodeling and repair (Lanyon, 1980). In the case of birds, avian femora R was also found to scale with slight negative allometry, although scatter was extremely high compared with previous studies (Cubo et al., 1999) and 95% confidence intervals included 1. Our results would suggest that scaling of curvature contributes little toward achieving mass-invariant safety factors.

Safety factors under bending typically fall between 3 and 20 (Table 7). Some individual bones, such as the heron (*Ardea cinerea*) femur and platypus (*Ornithorhynchus anatinus*) tibia, have safety factors of less than 1 under bending however, indicating that their hindlimbs could not support their body weight when statically loaded in horizontal bending. When compared with curved elements typically considered in engineering, vertebrate bones are relatively straight (as determined by R/r value), and application of eq. 5 to the estimation of F_b does not produce results significantly different to those of eq. 4. Safety factors under torsion are particularly low (Table 7), with several species possessing SF values of less than 1. However, the modeled load conditions are extreme and represent the condition where the bone is immobilized and a significant fraction of body weight acts with the lever arm of the alternative bone element. In practice, torsion is likely to be a minor contributor to total loading in mammal bones (although exceptions may exist in the limbs of small crouched mammals (Keller and Spengler, 1989; Butcher et al., 2011), and these results are unlikely to reflect the

TABLE 5. SMA Scaling exponents of maximum force against recorded/literature body mass

	a	*b*	95% CI	r^2	*P*
Compression					
MF	3.48	**0.74**	0.68–0.80	0.96	<0.001***
MT	3.37	**0.74**	0.67–0.80	0.94	<0.001***
BF	3.45	**0.82**	0.72–0.93	0.90	<0.001***
BT	3.40	**0.82**	0.75–0.89	0.95	<0.001***
Compression (incorporating curvature)					
MF	3.03	**0.67**	0.59–0.76	0.89	<0.001***
MT	2.74	**0.74**	0.64–0.85	0.86	<0.001***
BF	2.88	**0.92**	0.79–1.07	0.85	<0.001***
BT	2.83	**0.77**	0.66–0.90	0.85	<0.001***
Bending					
MF	1.78	**0.76**	0.70–0.82	0.95	<0.001***
MT	1.47	**0.80**	0.73–0.87	0.94	<0.001***
BF	1.83	**0.95**	0.82–1.11	0.86	<0.001***
BT	1.51	**0.88**	0.80–0.96	0.94	<0.001***
Bending (incorporating curvature)					
MF	1.78	**0.76**	0.70–0.82	0.96	<0.001***
MT	1.46	**0.80**	0.73–0.87	0.94	<0.001***
BF	1.83	**0.95**	0.82–1.10	0.86	<0.001***
BT	1.51	**0.88**	0.80–0.96	0.94	<0.001***
Torsion					
MF	1.32	**0.80**	0.73–0.87	0.95	<0.001***
MT	1.09	**0.76**	0.69–0.84	0.93	<0.001***
BF	1.20	**0.93**	0.79–1.09	0.83	<0.001***
BT	1.30	**0.89**	0.82–0.99	0.96	<0.001***

Regression statistics in the form $\log Y = a \log M_b^b$, where *Y* is calculated force (N) and M_b is body mass in kilograms. Slopes were fitted by means of model-II SMA regression. MF, mammal femur; MT, mammal tibia; BF, bird femur; BT, bird tibiotarsus. Scaling exponents are given in bold.

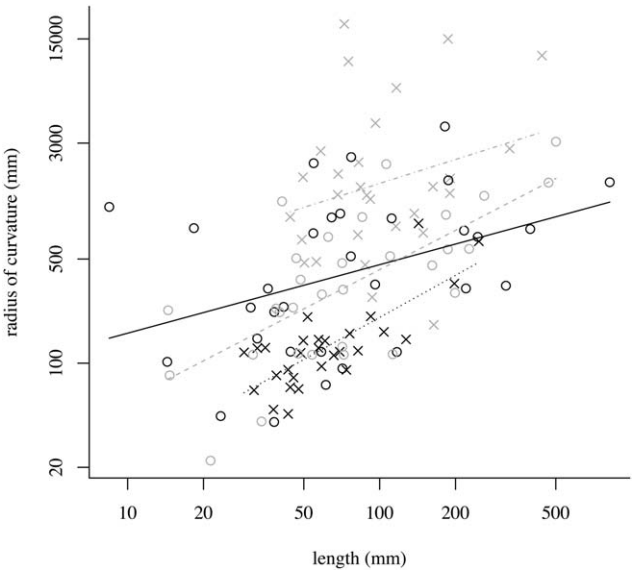

Fig. 6. Radius of curvature (mm) against bone length (mm). Black open circle, solid line, mammal femur; gray open circle, dashed line, mammal tibia; black cross, dotted line, bird femur; gray cross, dot-dash line, bird tibiotarsus. No significant relationship exists between bone length and radius of curvature in the bird tibiotarsus. Model-I OLS regression equations are mammal femur, $y = 1.74x^{0.46}$; mammal tibia, $y = 0.88x^{0.88}$; bird femur, $y = 0.43x^{0.94}$.

absolute values of torsion that occur during normal use. Furthermore, it is feasible that the particularly low safety factors calculated for the avian femur under torsion (Table 7) are a function of considering torsional lever arm to be proportional to the length of the particularly elongated avian tibiotarsus.

With the exception of the avian hindlimb under torsion, safety factors are lower in the zeugopodium than the stylopodium (Table 7). This may be explained by the well-documented phenomenon whereby the mass of bone contributes to the moment of inertia about the hip joint in proportion to the square of distance from the joint. Therefore, distal segments of the limb tend to be as light as possible to reduce the inertial forces needed to accelerate the leg during the stride, particularly in fast-moving cursors (Currey, 2003). This is reflected in an increased risk of fracture in the proximal-distal direction in the lower limbs (Van Staa et al., 2001).

Overall, these results provide further support for the hypothesis of postural modification as a effective means by which safety factors are maintained in terrestrial mammals (Biewener, 1989). Large mammals are functionally adapted to position their hindlimbs closer to vertical to achieve safety factors equal to those of small crouched mammals (Fig. 10). The heaviest mammals in this sample (*Elephas maximus* and *Giraffa camelopardalis*) are required to maintain values of θ close to 90 degree to achieve a static safety factor of 15 (*E. maximus* tibia fails to intersect safety factor line entirely; Fig. 8). Under unpredictable dynamic loading conditions, instantaneous peak stress values (and minimum θ) are likely to be significantly greater. The possibility of differential scaling of limb bone dimensions was not investigated here using separate regressions of bone dimensions against body mass in small and large individuals. Yet, it is clear that the potential to increase θ further is limited in large individuals, and stronger positive allometry of bone geometry may be necessary to maintain safety factors in very large extant and extinct vertebrates (Bertram and Biewener, 1990; Christiansen, 1999a,b; Chinnery, 2004). In the future, incorporating kinematic scaling (GRF and limb postural measurements during stance) with bone morphological scaling across a broad size range may illuminate this further. In particular, postural data from the >300-kg size range of mammals is needed to compliment existing morphological data before any "break point" in behavioral and skeletal scaling can be distinguished.

While for a given value of θ, a general trend of lower safety factors in larger mammals is apparent (Fig. 8), interesting exceptions exist. The femur of the cheetah (*Acinonyx jubatus*) is predicted to experience lower SF than that of an elephant (Fig. 8). This is probably due to the long, gracile nature of the element (Day and Jayne, 2007), and may function to increase stride length and maintain high duty factors (hence lower peak limb force) in this cursor while minimizing limb mass (Hudson et al., 2011). It is also possible that the safety factors in this species are lower than in other animals. In the mammal tibia, the lowest safety factor occurs in the platypus (*O. anatinus*). These semiaquatic monotremes posses specializations for swimming that negatively affect their terrestrial locomotion, and are restricted to a walking gait on land (Fish et al., 2001). Furthermore when walking at slow speeds, the ventral side of their body remains in contact with the ground, reducing the

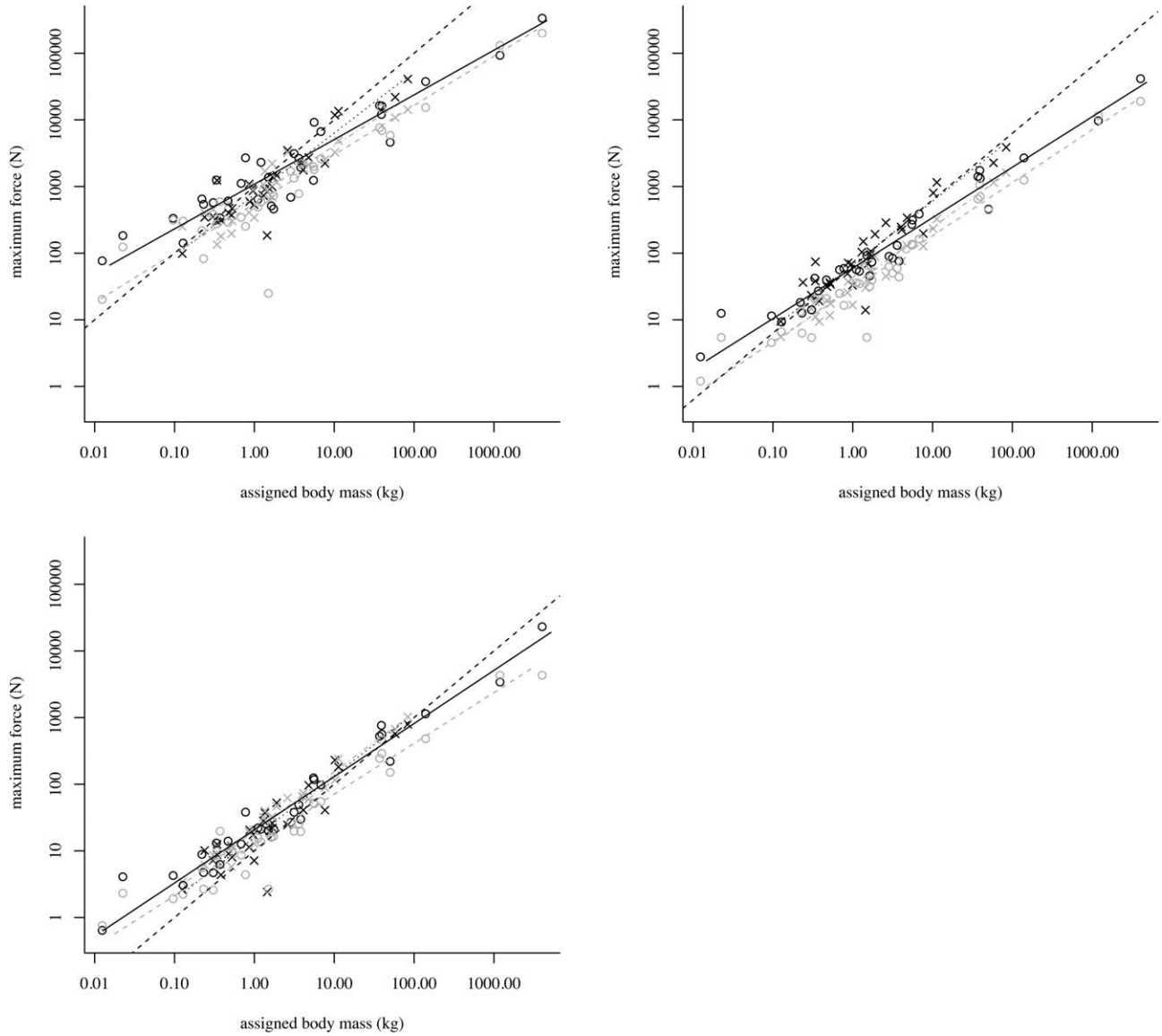

Fig. 7. SMA regressions of maximum resistible force before yield (N) against body mass (kg). Refer to Fig. 6 for symbols. (**a**) compressional loading regime (incorporating curvature); (**b**) bending loading regime (incorporating curvature); (**c**) torsional loading regime. Black dashed line reflects a slope value of 1. See Table 5 for slope values.

requirement for body mass to be supported by the limbs alone (Pridmore, 1985).

The safety factor curves of several small mammals fail to intersect lines representing safety factors of 12–20 (Fig. 8) for values of θ between 0 and 90 degree. These animals are able to operate at high safety factors, allowing them to adopt a crouched posture and abduction of the limbs (particularly the stylopodia) which would contribute significantly to bending loads (Blob and Biewener, 1999), as previously reported in several small mammals, including rodents, opossums, and mustelids (Jenkins, 1971; Gasc, 1993; Fischer, 1994). These results corroborate the interpretations of Reilly et al. (2007) for small crouched mammals, in which there was no significant change in EMA across the size range of 0.01–1 kg, with posture instead being maintained by relatively increasing the cross-sectional area of antigravity muscles.

Attempts at reconstructing the ancestral mode of locomotion used by early mammals have combined palaeontological and modern biomechanical data (Gasc, 2001). The high safety factors and significant degree of torsional loading present in the femur of the crouching marsupial, Virginia opossum (*Didelphis virginiana*), have been interpreted as characteristic of basal mammalian species (Butcher et al., 2011). Considerable bending of the limb bones in the mediolateral direction was also identified, and linked to anteroposteriorly flattened cross sections in basal therapsids (Blob, 2001). Here, predicted values of F_b and F_t (calculated in both AP and ML

TABLE 6. Test for common slopes between SMA regression slopes of maximum force against assigned body mass

	Compression	Bending	Torsion
	Test for common slope		
lr	10.01	10.09	8.70
P	0.02*	0.02*	0.03*

Compression and bending slopes incorporate effects of bone curvature. Likelihood ratios (lr) calculated for slopes. The null hypothesis (H_0) of a common slope/intercept is rejected when $P<0.05$.

directions) for the marsupial sugar glider (*Petaurus breviceps*), and the monotremes *O. anatinus* and the short-beaked echidna (*Tachyglossus aculeatus*) are not significant outliers in regressions of maximum force against body mass. The non-eutherian mammals included in this study do not possess robust hindlimbs (relative to eutharians) that would be indicative of significantly higher bending and torsional loads. In the absence of additional kinematic and morphometric data from quadrupedal, terrestrial/arboreal marsupials, and monotremes, the estimated levels of torsion and mediolateral bending in ancestral mammal limb loading remain unclear.

In line with previously published results (Cubo and Casinos, 1998; Doube et al., 2012), cross-sectional properties of avian hindlimbs scale more strongly than in corresponding mammalian limbs. Tibiotarsus length scales as $l \propto M_b^{0.38}$, higher than reported elsewhere (Prange et al., 1979; Olmos et al., 1996), but similar to that of Doube et al. (2012). In the absence of postural modifications, safety factors are still predicted to scale with body mass in the avian tibiotarsus despite positive allometric scaling of cross-sectional geometry. For a given safety factor, the value of θ_{max} in the bird tibiotarsus is absolutely higher, and scales to body mass more slowly than in mammal hindlimb bones (Fig. 10). To achieve constant tibiotarsal safety factors across their size range, this sample of birds are required to modify θ_{max} far less than mammal limb bones. From these results, we may hypothesize that in birds EMA does not scale around the knee as rapidly as recorded in mammals ($EMA \propto M_b^{0.24}$) (Biewener, 1989), although this remains to be tested with kinematic data.

In contrast to the wide arc of tibiotarsal retraction at the knee (50–80 degree), the avian femur typically rotates through less than 10 degree at the hip during the support phase at low/moderate speeds (Gatesy and Biewener, 1991). A knee-based retractor system and subhorizontal femur act to keep the center of mass positioned over the feet, which has shifted anteriorly following the reduction of tail length in the non-avian theropod lineage, matched by the shift from hip to knee-based limb flexure in avian theropods (Gatesy, 1995). That modern flightless birds have failed to attain maximum body masses comparable to those of non-avian theropods has previously been attributed to this subhorizontal femoral posture (Gatesy, 1991). The stylopodia of non-avian theropods have been found to scale differently to those of modern birds, suggesting they were subject to an alternative loading regime in which femora were oriented more parallel to the GRF. Axial loading of columnar limbs may therefore have facilitated the evolution of gigantism in the theropod lineage (Gatesy, 1991). In contrast, it has been suggested that the shift to a more horizontal femur has led to femoral scaling becoming a constraint on modern avian body size (Gatesy, 1991).

TABLE 7. Average safety factors (SF), ratios of safety factors between loading regimes, and test for the effect of phylogeny and skeletal element upon mean safety factors

	Compression	Bending	Torsion
SF			
BF	88.4	7.68	1.83
BT	76.2	3.37	2.01
MF	396.8	18.66	6.38
MT	209.3	9.17	4.13
Ratio			
BF	52.8	4.46	1
BT	35.8	1.68	1
MF	57.0	2.88	1
MT	52.6	2.50	1
Two-way ANOVA			
Phylogeny			
F	18.06	10.46	13.48
P	<0.001***	0.002**	<0.001***
Element			
F	3.92	7.26	1.40
P	0.05*	0.008**	0.24
Interaction			
F	2.85	0.99	1.81
P	0.09	0.32	0.18
Post hoc Tukey test (*P*)			
MF:MT	0.05*	0.05*	0.29
BF:BT	0.99	0.66	0.99
MF:BF	<0.001***	0.02*	0.003**
MT:BT	0.27	0.39	0.36
MF:BT	<0.001***	<0.001***	0.005**
MT:BF	0.36	0.97	0.28

The effect of phylogenetic grouping and skeletal element on mean safety factors is tested in a two-way ANOVA. A post hoc Tukey test of multiple means indicates pairwise comparisons that are significantly different. Asterisks denote level of significance: *$P<0.05$; **$P<0.01$; ***$P<0.001$. MF, mammal femur; MT, mammal tibia; BF, bird femur; BT, bird tibiotarsus.

However, here, we find bird femora scale with extreme robusticity, with $d_{AP} \propto l^{1.24}$ and $I_{AP} \propto l^{4.91}$ (Table 2). As a result, force scales close to isometry with body mass across all loading regimes, and constant safety factors in the subhorizontal femur may be achieved via scaling of bone geometry alone. Postural constraints do not appear to be the limiting factor in modern bird size, and may instead be attributed to the problems associated with contact incubation (Birchard and Deeming, 2009). The avian eggshell reflects a compromise between strength against the forces of parental body mass acting during incubation, and fragility necessary for the developed chick to successfully hatch. Safety factors for eggshell breakage have been shown to scale negatively against body mass (Ar and Rahn, 1979) assuming contact incubation. However, further work incorporating both morphometric and kinematic datasets is needed before the hypothesis of mass-invariant safety factors in the avian femur can be confidently accepted.

When plotting species-specific curves of maximum SF against θ in avian hindlimbs (Fig. 9), the lowest safety factors are not always associated with the heaviest

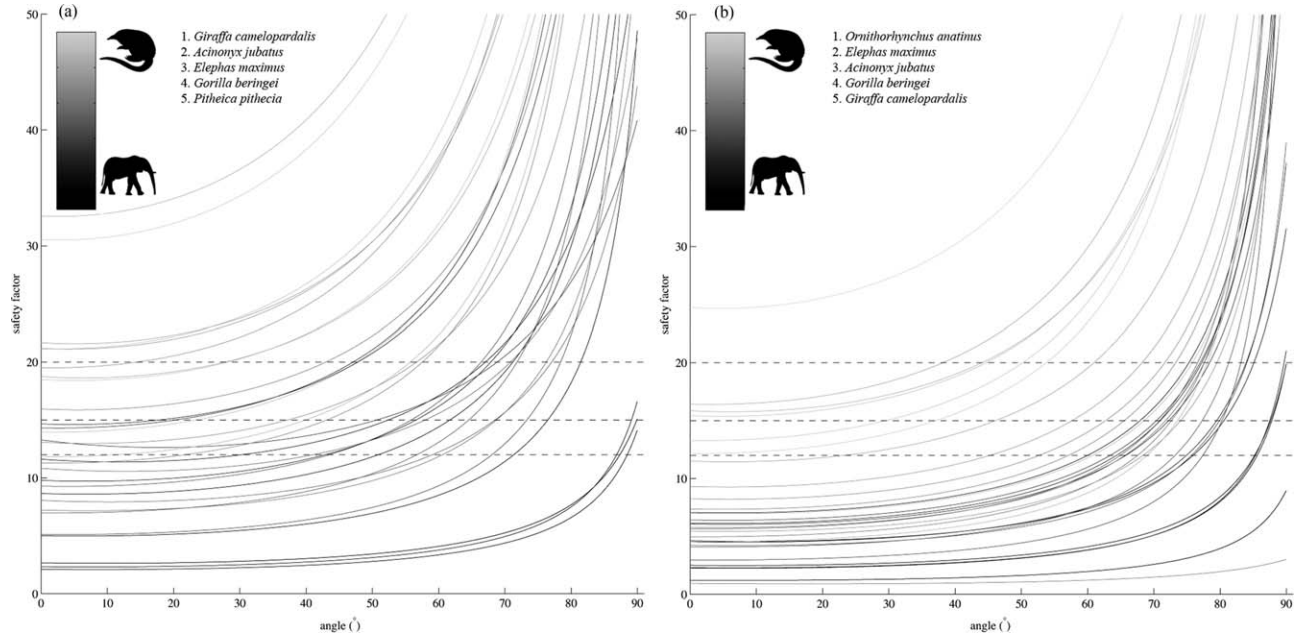

Fig. 8. Mammal species-specific curves of combined force (F_{cb}) against angle from the horizontal (θ) in degrees. (**a**) mammal femur; (**b**) mammal tibia. Dashed horizontal lines represent safety factors of 12, 15, and 20, respectively. Shade of individual curve follows gradient from black (heaviest individual) to light gray (lightest individual). Top five species possessing lowest safety factors under bending are listed.

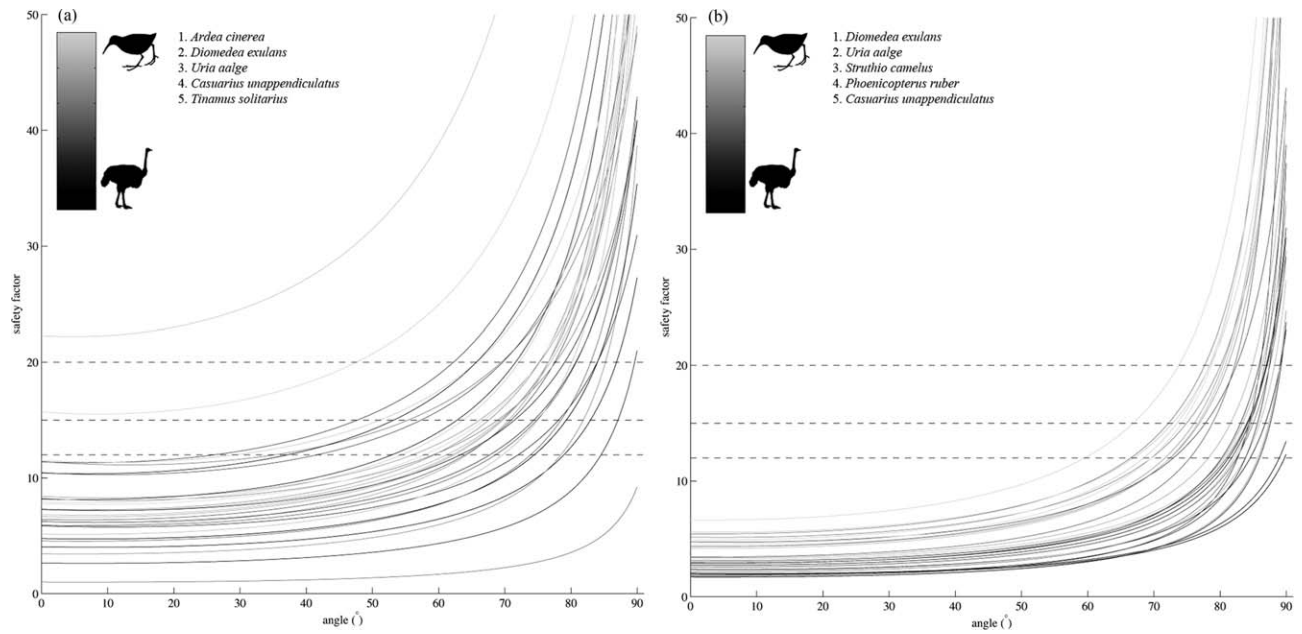

Fig. 9. Bird species-specific curves of combined force (F_{cb}) against angle from horizontal (θ) in degrees. (**a**) bird femur; (**b**) bird tibiotarsus. Annotations follow those of Fig. 8.

flightless birds in the sample (*Struthio camelus, Casuarius unappeniculatus, Raphus cucullatus*, and *Pezophaps solitaria*). Instead, low values of SF are associated with wading birds (*Ardea cinerea, Phoenicopterus ruber*), diving birds (*Uria aalge*), and long-distance dynamic soarers (*Diomeda exulans*). The shift away from cursoriality toward specialized locomotor groups appears to be characterized by a decrease in safety factors in avian hindlimbs. Unlike mammals, in which the largest species tend to experience the lowest safety factors (based on bone geometry alone; Fig. 8), a strong behavioral signal may also be present in birds.

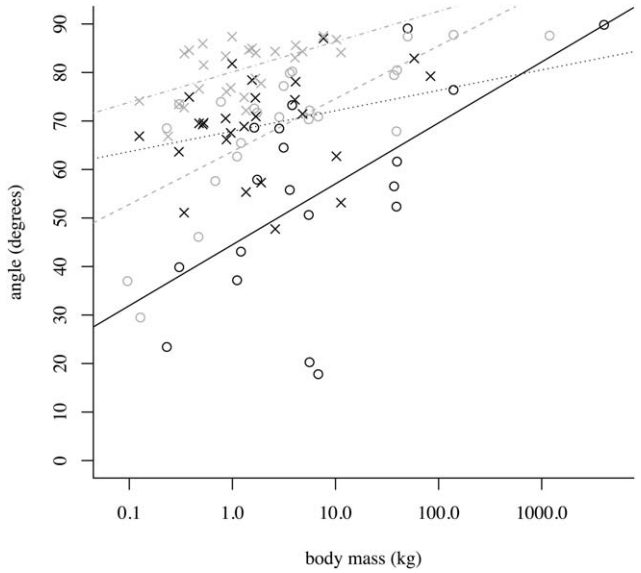

Fig. 10. Bone angle (θ) scales with body mass. Refer to Fig. 6 for symbols. The minimum angle from horizontal at which a bone may be held statically when subject to combined compressive and bending force, while maintaining a safety factor of 15, scales significantly with M_b (with the exception of the avian femur). Model-I OLS regression equations are: mammal femur, $y=44.5x^{12.6}$; mammal tibia, $y=63.7x^{10.9}$; bird femur, $y=67.9x^{4.21}$ (not significantly different from zero; $P>0.07$); bird tibia, $y=80.1x^{6.26}$. When individual species curves do not intersect the safety factor line (see Figs. 10 and 9), they are not included in the analysis.

There are a number of important considerations of the analysis presented above. In common with most analyses of bone loading, we calculate values for maximum resistible force before yield and θ_{max} using static loading models. Even analyses such as EMA, in which the magnitude and direction of the instantaneous GRF at midstance are measured, are considered static analyses as they ignore any loading associated with the relative accelerations of each limb segment. During locomotion, peak stresses experienced within bones are due to muscle contractions, rather than the effects of gravity (Rubin and Lanyon, 1984; Biewener, 1991). It therefore follows that muscle forces should primarily determine bone dimensions, rather than static loads (Kokshenev et al., 2003). Here, we find the maximum static force a bone is capable of withstanding scales to body mass with negative allometry ($F \propto M_b^{0.67-0.89}$, with the exception of the avian femur), and interpret this as a decrease in safety factor with size. However, experimental results suggest peak muscle force scales to body mass approximately as $M_b^{0.8}$ (Alexander et al., 1981). Therefore, if bone allometry is coupled with muscle force allometry, it appears constant safety factors to peak muscle force may be frequently achieved via scaling of bone geometry alone.

In addition, predicted values of F_b were calculated using Euler-Bernoulli simple beam theory, in which potential deformation caused by shear is ignored (Gere and Goodno, 2012). Standard engineering practice suggests that that beam theory equations are reasonably accurate only for objects with an aspect ratio (l:d) of 16 or greater (Turner and Burr, 1993), which is only sometimes the case for long bones. Roughly half the present sample have a l:d of less than 16, and a greater proportion of total σ under bending will consist of shear stress. F_b may be better approximated by the less frequently used Timoshenko beam theory, in which shear deformations are included (Gere and Goodno, 2012). Further work is needed to understand the magnitude of errors associated with ignoring shear deformations, and FEA may be a useful computational tool for such analyses (Brassey et al., 2013).

CONCLUSIONS

Scaling of cross-sectional geometry alone does not achieve mass-invariant safety factors in mammalian hindlimbs. The angle from vertical at which mammals must hold their limb bones to achieve stress similarity scales significantly with body mass. In contrast, more extreme positive allometry in the avian femur may be capable of preventing safety factors from decreasing with body size. If constant safety factors are maintained in the subhorizontal avian theropod femur, this postural constraint does not appear to act as a limiting factor on maximum body size. The theory of postural adjustment to maintain safety factors is broadly supported on an order-level in mammals. However, idiosyncratic behavioral and locomotor signals are found to overlay frequently the relationship between force, bone angle, and body mass, particularly in birds. The applicability of EMA scaling to birds, and outside the sprawling rodent-erect ungulate dichotomy in mammals, remains to be tested.

ACKNOWLEDGEMENTS

The authors are grateful to the staff of the Henry Moseley X-ray Imaging Facility, University of Manchester; Professor Paul Mummery, Dr Tristan Lowe; The University of Liverpool Small Animal Hospital: Martin Baker; Manchester Museum: Henry McGhie, Judith White; Liverpool World Museum: Tony Parker. The comments of two anonymous reviewers were very useful in refining the manuscript.

LITERATURE CITED

Agnarsson I, Kuntner M, May-Collado LJ. 2010. Dogs, cats, and kin: a molecular species-level phylogeny of Carnivora. Mol Phylogenet Evol 54:726–745.

Alexander RMN. 1974. The mechanics of jumping by a dog (Canis familiaris). J Zool 173:549–573.

Alexander, RMN. 1981. Factors of safety in the structure of Animals. Sci Prog 67:109–130.

Alexander RMN. 1989. Dynamics of Dinosaurs and Other Extinct Giants. New York: Columbia University Press.

Alexander RMN, Jayes AS. 1983. A dynamic similarity hypothesis for the gaits of quadrupedal mammals. J Zool 201:135–152.

Alexander RMN, Pond C. 1992. Locomotion and bone strength of the white rhinoceros, Ceratotherium simum. J Zool 227:63–69.

Alexander RMN, Jayes AS, Maloiy GMO, Wathuta EM. 1981. Allometry of the leg muscles of mammals. J Zool 194:539–552.

Angst D, Buffetaut E, Abourachid A. 2011. The end of the fat dodo? A new mass estimate for Raphus cucullatus. Naturwissenschaften 98:233–236.

Ar A, Rahn H. 1979. The avian egg: mass and strength. The Condor 81:331–337.

Arnold C, Matthews LJ, Nunn CL. 2010. The 10kTrees website: a new online resource for primate phylogeny. Evol Anthropol 19:114–118.

Beck R. 2008. A dated phylogeny of marsupials using a molecular supermatrix and multiple fossil constraints. J Mammal 89:175–189.
Bertram J, Biewener A. 1988. Bone curvature: sacrificing strength for load predictability? J Theor Biol 131:75–92.
Bertram J, Biewener A. 1990. Differential scaling of the long bones in the terrestrial Carnivora and other mammals. J Morphol 204:157–169.
Bertram J, Biewener A. 1992. Allometry and curvature in the long bones of quadrupedal mammals. J Zool 226:455–467.
Biewener A. 1982. Bone strength in small mammals and bipedal birds: do safety factors change with body size? J Exp Biol 98:289–301.
Biewener A. 1983. Allometry of quadrupedal locomotion: the scaling of duty factor, bone curvature and limb orientation to body size. J Exp Biol 105:147–171.
Biewener A. 1989. Scaling body support in mammals: limb posture and muscle mechanics. Science 245:45–48.
Biewener A. 1991. Musculoskeletal design in relation to body size. J Biomech 24:19–29.
Biewener A. 2005. Biomechanical consequences of scaling. J Exp Biol 208:1665–1676.
Birchard G, Deeming D. 2009. Avian eggshell thickness: scaling and maximum body mass in birds. J Zool. 279:95–101.
Blanga-Kanfi S, Miranda H, Penn O, Pupko T, DeBry RW, Huchon D. 2009. Rodent phylogeny revised: analysis of six nuclear genes from all major rodent clades. BMC Evol Biol 9:71.
Blob R. 2001. Evolution of hindlimb posture in nonmammalian therapsids: biomechanical tests of paleontological hypotheses. Paleobiology 27:14–38.
Blob R, Biewener A. 1999. In vivo locomotor strain in the hindlimb bones of Alligator mississippiensis and Iguana iguana: implications for the evolution of limb bone safety factor and non-sprawling limb posture. J Exp Biol 202:1023–1046.
Blob R, Biewener A. 2001. Mechanics of limb bone loading during terrestrial locomotion in the green iguana (Iguana iguana) and American alligator (Alligator mississippiensis). J Exp Biol 204:1099–1122.
Boresi AP, Schmidt RJ. 2002. Advanced Mechanics of Materials. 6th ed. New Jersey: John Wiley & Sons.
Brassey CB, Margetts L, Kitchener AC, Withers PJ, Manning PL, Sellers WI. 2013. Finite element modelling versus simple beam theory: comparing methods for estimating stress in a diverse sample of vertebrate long bones. J R Soc Interface 10: 20120823.
Brown JR, Rest JS, Garcia-Moreno J, Sorenson MD, Mindell DP. 2008. Strong mitochondrial DNA support for a Cretaceous origin of modern avian lineages. BMC Biol 6:6.
Butcher M. White B. Hudzik N. 2011. In vivo strains in the femur of the Virginia opossum (Didelphis virginiana) during terrestrial locomotion: testing hypotheses of evolutionary shifts in mammalian bone loading and design. J Exp Biol 214:2631–2640.
Campione NE, Evans DC. 2012. A universal scaling relationship between body mass and proximal limb bone dimensions in quadrupedal terrestrial tetrapods. BMC Biol 10:60.
Cezayirlioglu H, Bahnuik E, Davy DT, Heiple KG. 1985. Anisotropic yield behavior of bone under combined axial force and torque. J Biomech 18:61–69.
Chinnery B. 2004. Morphometric analysis of evolutionary trends in the ceratopsian postcranial skeleton. J Vert Paleo 24:591–609.
Christiansen P. 1998. Strength indicator values of theropod long bones, with comments on limb proportions and cursorial potential. Gaia 15:241–255.
Christiansen P. 1999a. Long bone scaling and limb posture in non-avian theropods: evidence for differential allometry. J Vert Paleo 19:666–680.
Christiansen P. 1999b. Scaling of the limb long bones to body mass in terrestrial mammals. J Morphol 239:167–190.
Clemente CJ, Withers PC, Thompson G, Lloyd D. 2011. Evolution of limb bone loading and body size in varanid lizards. J Exp Biol 214:3013–3020.
Cubo J, Casinos A. 2000. Mechanical properties and chemical composition of avian long bones. Eur J Morphol 38:112–121.
Cubo J, Casinos A. 1998. The variation of the cross-sectional shape in the long bones of birds and mammals. Ann Sci Nat Zool 19:51–62.
Cubo J, Menten L, Casinos A. 1999. Sagittal long bone curvature in birds. Ann Sci Nat Zool 20:153–159.
Currey JD. 2002. Bones: Structure and Mechanics. Oxford: Princeton University Press.
Currey JD. 2003. How well are bones designed to resist fracture? J Bone Miner Res 18:591–598.
Davies SJJF. 2002. Ratites and Tinamous. Oxford: Oxford University Press.
Davies SJJF. 2003. Ratites. In: Hutchins M, editor. Grzimek's Animal Life Encyclopedia, Volume 8: Tinamous and Ratites. Farmington Hills, MI: Gale Group. p 89–90.
Day L, Jayne B. 2007. Interspecific scaling of the morphology and posture of the limbs during the locomotion of cats (Felidae). J Exp Biol 210:642–654.
Decker J, Pires JC, Conant GC, McKay SD, Heaton MP, Chen K, Cooper A, Vilkki J, Seabury CM, Caetano AR et al. 2009. Resolving the evolution of extant and extinct ruminants with high-throughput phylogenomics. PNAS 106:18644–18649.
Demes B, Jungers WL. 1993. Long-bone cross-sectional dimensions, locomotor adaptations and body-size in prosimian primates. J Hum Evol 25:57–74.
Demes B, Larson SG, Stern JT, Jr., Jungers WL, Biknevicius AR, Schmitt, D. 1994. The kinetics of primate quadrupedalism. J Hum Evol 26:353–374.
do Amaral FR, Sheldon FH, Gamauf A, Haring E, Riesing M, Silveira LF, Wajntal, A. 2009. Patterns and processes of diversification in a widespread and ecologically diverse avian group, the buteonine hawks (Aves, Accipitridae). Mol Phylogenet Evol 53:703–715.
Doube M, Klosowski M, Arganda-Carreras I. 2010. BoneJ: free and extensible bone image analysis in ImageJ. Bone 47:1076–1079.
Doube M, Yen SCW, Klosowski MM, Farke AA, Hutchinson JR, Shefelbine, SJ. 2012. Whole-bone scaling of the avian pelvic limb. J Anatomy 221:21–29.
Dunning JB. 1993. CRC Handbook of Avian Body Mass. Boca Raton: CRC Press.
Economos A. 1983. Elastic and/or geometric similarity in mammalian design? J Theor Biol 103:167–172.
Eizirik E, Murphy WJ, Koepfli KP, Johnson WE, Dragoo JW, Wayne RK, O'Brian SJ. 2010. Pattern and timing of diversification of the mammalian order Carnivora inferred from multiple nuclear gene sequences. Mol Phylogenet Evol 56:49–63.
Erickson G, Catanese J III, Keaveny T. 2002. Evolution of the biomechanical material properties of the femur. Anat Rec 268:115–124.
Fain M, Krajewski C, Houde P. 2007. Phylogeny of "'core Gruiformes'" (Aves: Grues) and resolution of the Limpkin–Sungrebe problem. Mol Phylogenet Evol, 43:515–529.
Felsenstein J. 1988. Phylogenies and quantitative characters. Annu Rev Ecol Syst 19:445–471.
Fischer M. 1994. Crouched posture and high fulcrum, a principle in the locomotion of small mammals: the example of the rock hyrax (Procavia capensis)(Mammalia: Hyracoidea). J Hum Evol 26:501–524.
Fish F, Frappell PB, Baudinette RV, MacFarlane PM. 2001. Energetics of terrestrial locomotion of the platypus Ornithorhynchus anatinus. J Exp. Biol. 204:797–803.
Gambaryan PP. 1976. How Mammals Run. New York: John Wiley & Sons Inc.
Garcia G, da Silva J. 2004. On the scaling of mammalian long bones. J Exp Biol 207:1577–1584.
Garcia G, da Silva J. 2006. Interspecific allometry of bone dimensions: a review of the theoretical models. Phys Life Rev 3:188–209.
Gartner GEA, Hicks JW, Manzani PR, Andrade DV, Abe AS, Wang T, Secor SM, Gardland T, Jr. 2010. Phylogeny, ecology, and heart position in snakes. Physiol Biochem Zool 83:43–54.
Gasc JP. 1993. Asymmetrical gait of the Saharian rodent Meriones shawi shawi (Duvernoy, 1842) (Rodentia, Mammalia): a high-speed cineradiographic analysis. Can J Zool 71:790–798.
Gasc JP. 2001. Comparative aspects of gait, scaling and mechanics in mammals. Comp Biochem Phys A 131:121–133.

Gatesy S. 1991. Hind limb scaling in birds and other theropods: implications for terrestrial locomotion. J Morph 209:83–96.
Gatesy S. 1995. Functional evolution of the hindlimb and tail from basal theropods to birds. In: Thomason JJ, editor. Functional Morphology in Vertebrate Palaeontology. Cambridge: Cambridge University Press. p 219–234.
Gatesy S, Biewener A. 1991. Bipedal locomotion: effects of speed, size and limb posture in birds and humans. J Zool 224:127–147.
Gere JM, Goodno BJ. 2012. Mechanics of Materials. Stamford: Cengage Learning.
Gonzalez J, Düttmann H, Wink M. 2009. Phylogenetic relationships based on two mitochondrial genes and hybridization patterns in Anatidae. J Zool. 279:310–318.
Hackett S, Kimball RT, Reddy S, Bowie RCK, Braun EL, Braun MJ, Chojnowski JL, Cox WA, Han KL, Harshman J et al. 2008. A phylogenomic study of birds reveals their evolutionary history. Science 320:1763–1767.
Hudson PE, Corr SA, Payne-Davis RC, Clancy SN, Lane E, Wilson AM. 2011. Functional anatomy of the cheetah (Acinonyx jubatus) hindlimb. J Anat 218:363–374.
Hutchinson JR, Famini D, Lair R, Kram R. 2003. Are fast-moving elephants really running? Nature 422:493–494.
Jenkins F. 1971. Limb posture and locomotion in the Virginia opossum (Didelphis marsupialis) and in other non-cursorial mammals. J Zool 165:303–315.
Keller TS, Spengler DM. 1989. Regulation of bone stress and strain in the immature and mature rat femur. J Biomech 22:1115–1127.
Kokshenev V, Silva J, Garcia G. 2003. Long-bone allometry of terrestrial mammals and the geometric-shape and elastic-force constraints of bone evolution. J Theor Biol 224:551–556.
Lanyon LE. 1980. The influence of function on the development of bone curvature. An experimental study on the rat tibia. J Zool 192:457–466.
Lavin SR, Karasov WH, Ives AR, Middleton KM, Garland T, Jr. 2008. Morphometrics of the avian small intestine compared with that of nonflying mammals: A Phylogenetic Approach. Physiol Biochem Zool 81:526–550.
Livezey B. 1993. An ecomorphological review of the dodo (Raphus cucullatus) and solitaire (Pezophaps solitaria), flightless Columbiformes of the Mascarene Islands. J Zool 230:247–292.
Matthee CA, van Vuuren BJ, Bell D, Robinson TJ. 2004. A molecular supermatrix of the rabbits and hares (Leporidae) allows for the identification of five intercontinental exchanges during the Miocene. Syst Biol 53:433–447.
McArdle BH. 1988. The structural relationship—regression in biology. Can J Zool 66:2329–2339.
McMahon T. 1973. Size and shape in biology: elastic criteria impose limits on biological proportions, and consequently on metabolic rates. Science 179:1201–1204.
McMahon T. 1975. Allometry and biomechanics: limb bones in adult ungulates. Am Nat 109:547–563.
Olmos M, Casinos A, Cubo J. 1996. Limb allometry in birds. Ann Sci Nat Zool 17:39–49.
Pereira S, Baker A. 2006. A molecular timescale for galliform birds accounting for uncertainty in time estimates and heterogeneity of rates of DNA substitutions across lineages and sites. Mol Phylogenet Evol 38:499–509.
Pereira S, Baker A. 2008. DNA evidence for a Paleocene origin of the Alcidae (Aves: Charadriiformes) in the Pacific and multiple dispersals across northern oceans. Mol Phylogenet Evol 46:430–445.
Pereira S, Johnson KP, Clayton DH, Baker AJ. 2007. Mitochondrial and nuclear DNA sequences support a Cretaceous origin of Columbiformes and a dispersal-driven radiation in the Paleogene. Syst Biol 56:656–672.
Phillips MJ, Gibb GC, Crimp EA, Penny D. 2010. Tinamous and moa flock together: mitochondrial genome sequence analysis reveals independent losses of flight among ratites. Syst Biol 59:90–107.
Polk J. 2002. Adaptive and phylogenetic influences on musculoskeletal design in cercopithecine primates. J Exp Biol 205:3399–3412.
Prange H, Anderson J, Rahn H. 1979. Scaling of skeletal mass to body mass in birds and mammals. Am Nat 113:103–122.
Prasad A, Allard M. 2008. Confirming the phylogeny of mammals by use of large comparative sequence data sets. Mol Bio Evol 25:1795–1808.
Pridmore PA. 1985. Terrestrial locomotion in monotremes (Mammalia, Monotremata). J Zool 205:53–73.
Reilly SM, Willey JS, Biknevicius AR, Blob RW. 2005. Hindlimb function in the alligator: integrating movements, motor patterns, ground reaction forces and bone strain of terrestrial locomotion. J Exp Biol 208:993–1009.
Reilly SM, McElroy EJ, Biknevicius AR. 2007. Posture, gait and the ecological relevance of locomotor costs and energy-saving mechanisms in tetrapods. Zoology 110:271–289.
Ren L, Miller CE, Lair R, Hutchinson JR. 2010. Integration of biomechanical compliance, leverage, and power in elephant limbs. PNAS 107:7078–7082.
Roark RJ. 1965. Formulas for Stress and Strain. 4th ed. London: McGraw-Hill.
Rocha-Barbosa O, Casinos A. 2011. Geometry and evolutionary parallelism in the long bones of cavioid rodents and small artiodactyls. J Biosci 36:887–895.
Rowe T, Rich TH, Vickers-Rich T, Springer M, Woodburne MO. 2008. The oldest platypus and its bearing on divergence timing of the platypus and echidna clades. PNAS 105:1238–1242.
Rubin C, Lanyon L. 1982. Limb mechanics as a function of speed and gait: a study of functional strains in the radius and tibia of horse and dog. J Exp Biol 101:187–211.
Rubin C, Lanyon L. 1984. Dynamic strain similarity in vertebrates; an alternative to allometric limb bone scaling. J Theor Biol 107:321–327.
Schmitt D, Cartmill M, Griffin TM, Hanna JB, Lemelin P. 2006. Adaptive value of ambling gaits in primates and other mammals. J Exp Biol 209:2042–2049.
Seiffert E. 2007. A new estimate of afrotherian phylogeny based on simultaneous analysis of genomic, morphological, and fossil evidence. BMC Evol Biol 7:224.
Silva M, Downing JA. 1995. CRC Handbook of Mammalian Body Masses. Boca Raton: CRC Press.
Smithers RNH. 1983. The Mammals of the Southern African Subregion. Pretoria: University of Pretoria.
Springer MS, Murphy WJ, Eizirik E, O'Brien SJ. 2003. Placental mammal diversification and the Cretaceous–Tertiary boundary. PNAS 100:1056–1061.
Tumarkin-Deratzian AR, Vann DR, Dodson P. 2006. Bone surface texture as an ontogenetic indicator in long bones of the Canada goose Branta canadensis (Anseriformes : Anatidae). Zool J Linn Soc 148:133–168.
Turner C, Burr D. 1993. Basic biomechanical measurements of bone: a tutorial. Bone 14:595–608.
Van Staa TP, Dennison EM, Leufkens HGM, Cooper C. 2001. Epidemiology of fractures in England and Wales. Bone 29:517–522.
Warton DI, Wright IJ, Falster DS, Westoby M. 2006. Bivariate line-fitting methods for allometry. Biol Rev 81:259–291.
Wisconsin National Primate Research Centre. 2011. Primate Info Net: Primate Factsheets. Available at: http://pin.primate.wisc.edu/factsheets/ [Accessed 2011].
Woodburne M, Rich T, Springer M. 2003. The evolution of tribospheny and the antiquity of mammalian clades. Mol Phylogenet Evol 28:360–385.
Wright T, Schirtzinger EE, Matsumoto T, Eberhard JR, Graves GR, Sanchez JJ, Capelli S, Muller H, Scharpegge J, Chambers GK and Fleischer RC. 2008. A multilocus molecular phylogeny of the parrots (Psittaciformes): support for a Gondwanan origin during the Cretaceous. Mol Biol Evol 25:2141–2156.
Zioupos P. Currey JD, Casinos A. 2000. Exploring the effects of hypermineralisation in bone tissue by using an extreme biological example. Connect Tissue Res 41:229–248.